Materials Today Electronics 6 (2023) 100071

Contents lists available at ScienceDirect

Materials Today Electronics

journal homepage: www.elsevier.com/locate/mtelec

Review

Bio-inspired visual systems based on curved image sensors and synaptic devices

Zhenghao Long [a], Yucheng Ding [a], Swapnadeep Poddar [a], Leilei Gu [b,c], Qianpeng Zhang [a], Zhiyong Fan [a,c,*]

[a] Department of Electronic and Computer Engineering, The Hong Kong University of Science and Technology, Clear Water Bay, Kowloon, Hong Kong SAR, China
[b] Qingyuan Research Institute, School of Electronic Information and Electrical Engineering, Shanghai Jiao Tong University, No. 800 Dongchuan Road, 200240, Shanghai, PR China
[c] Shanghai Artificial Intelligence Laboratory, Shanghai, PR China

ARTICLE INFO

Keywords:
Bionic eyes
Curved image sensors
Photonic synapses

ABSTRACT

Vision is our dominant sense and is also highly desired in artificial systems. In this article, we provide an overview of bio-inspired visual systems that utilize curved image sensors and/or photonic synapses. The use of curved detector geometry ensures clear image sensing abilities with fewer optical elements, which has the potential to lead to miniaturization. Additionally, photonic synapses that integrate light sensing and neuromorphic preprocessing can reduce redundant modules and signal communications. This results in decreased device size and energy consumption. In this review, we begin by summarizing the fabrication processes of curved image sensors, followed by a review of typical bionic eye systems. Next, we discuss the materials and device structures of typical photonic synapses and related imaging systems. We also review the combinations of curved image sensors and photonic synapses. Finally, we summarize the key advantages and challenges of current bio-inspired visual systems.

Introduction

Sensing and computing of light information are crucial in biological and artificial systems. Although conventional artificial visual systems based on CCDs and CMOS image sensors have been well developed with high resolution and fast frame rates, planar CCD and CMOS-based systems still suffer from optical aberration and energy consumption-related problems. In recent years, the advent of bio-inspired devices, which can emulate efficient biological visual attributes in artificial hardware, has opened up possibilities for substantial enhancements to artificial visual systems.

Fig. 1 presents a comparison between conventional and bio-inspired visual systems. A typical conventional camera primarily consists of multiple lenses, a planar image sensor, and signal processing units. The lens system collects and focuses light onto the image sensors. Since a single glass lens often leads to significant geometric and chromatic aberration issues, multiple lenses are employed to mitigate these aberrations and produce high-quality images [1–3]. The image sensor is a planar silicon chip comprised of millions of pixels. Each pixel has the ability to detect local illumination and convert it into electrical signals. As a result, visual information from the environment can be detected and interpreted by electronic devices. These electrical signals are subsequently relayed to processing units, which undertake various tasks to transform the raw data into a clear, well-structured digital images. The aforementioned architecture brings with it several limitations. The use of multiple lenses significantly increases both weight and space occupancy. While the application of multiple lenses does suppress aberrations to some degree, spatial variation aberration remains challenges in optics [4,5]. For instance, it contributes to issues related to border aberration. Conversely, the design of a conventional camera is based on separating the sensing and processing units, which leads to unnecessary increase in terms of size and weight. Additionally, the redundant signal communication between functional modules significantly increases energy consumption [6]. In essence, modern artificial visual systems are hindered by inefficiencies in optical and computational characteristics, a predicament largely rooted in their architecture. As artificial intelligence applications continue to evolve, there is an escalating demand for the creation of advanced visual systems that can overcome these

* Corresponding author at: Department of Electronic and Computer Engineering, The Hong Kong University of Science and Technology, Clear Water Bay, Kowloon, Hong Kong SAR, China.
E-mail address: eezfan@ust.hk (Z. Fan).

https://doi.org/10.1016/j.mtelec.2023.100071
Received 4 June 2023; Received in revised form 4 October 2023; Accepted 15 October 2023
Available online 19 October 2023

inherent constraints and exhibit enhanced capabilities.

Evolution has given rise to remarkable eye structures capable of detecting and processing visual information, facilitating the routine activities of humans and other animals [7]. In recent years, various bio-inspired devices have been developed to address the problems of optical aberration and redundancy in traditional visual systems. Achieving low-aberration imaging necessitates resolving the geometrical mismatch between planar image sensors and Petzval field curvature. Many biological visual systems feature curved detector geometry, such as the human eye's hemispherical retina, which facilitates low aberration vision with minimal optical elements [8]. Drawing inspiration from the human eye, an ideal miniaturized artificial visual system would incorporate a few optical elements and a curved image sensor that aligns with the Petzval field curvature, making significant strides in imaging technology [9]. Furthermore, replacing flat image sensors with curved ones can enhance the field of view (FoV). In 2008, the world's first electronic eye camera, based on a hemispherical image sensor, was reported [10]. This innovation paved the way for the widespread reporting of bio-inspired visual systems based on curved image sensors over the past decades, prompting the development of new methods for non-planar fabrication. Primarily, there are two ways to fabricate a curved image sensor. One approach exploits the benefits of traditional microfabrication technologies, synthesizing pixel arrays on a planar substrate before transferring the pattern to a curved geometry [10–20]. This method facilitates reliable integration between photo sensing units and circuits, but due to stress issues during the deformation process, it is challenging to simultaneously achieve high pixel density and high curvature. Alternatively, photosensitive materials can be directly fabricated on curved geometry, avoiding the aforementioned stress issues [21–24]. However, fabricating high-density circuits on non-planar substrates remains a challenge.

Leveraging curved image sensors, innovative biomimetic eye devices have been developed. Bionic eyes, which emulate the effective structures and impressive capabilities of human eyes, have been widely reported. Often, a simple structure combining a single convex lens with a curved image sensor can achieve low aberration vision with an extensive FoV [10,14–16,22]. Additionally, the remarkable optical adaptivity of the human eye has been emulated in bio-inspired devices through integration with tunable optics [19,23]. Beyond human vision, bio-inspired visual systems that draw inspiration from other animals have been crafted with unique abilities, including thermal vision, amphibious vision, and an ultra-wide FoV [13,17,18,24]. Bio-inspired designs based on curved image sensors show promise in enhancing the imaging capability and environmental adaptability of artificial visual systems, thereby expanding potential application scenarios.

In addition to imaging capabilities, both biological and artificial systems critically depend on efficient signal processing. Unlike traditional artificial visual systems that depend on redundant processing units, animals process visual information effectively through neuron arrays present in their primary sensing organs and brains. The advent of photonic synapse devices that mimic neuronal memory and processing functions has enabled features of near-device and in-device computing [6]. In biological neurons, an action potential can modulate the synaptic weight, referring to the connection strength between the pre-synapse and post-synapse. This capacity to alter synaptic weight, defined as synaptic plasticity, forms the basis of learning, memory, and forgetting processes in the brain [25]. Synaptic plasticity primarily comprises Short-term Plasticity (STP) and Long-term Plasticity (LTP) [26]. In recent years, there has been a proliferation in the reporting of photonic synapses that exhibit synaptic plasticity under optical stimuli [26–43]. Both two-terminal and three-terminal device architectures have been developed. Two-terminal devices, capable of basic synaptic functions like STP and LTP, offer advantages in terms of large-scale integration in high-density crossbar array architectures [35]. Conversely, the phototransistor architecture, while also effectively emulating STP/LTP synaptic traits, has the added advantage of facilitating simultaneous signal relay and learning [40]. Leveraging their efficient in-device neuromorphic computing capabilities, synaptic devices find extensive use in a wide range of artificial intelligence (AI) related applications, including pattern recognition [37], color distinguishing [44] and motion detection [45,46].

Miniaturized, lightweight, energy-efficient, and high-performance visual systems are desirable in future visual prosthetic and machine vision applications [47,48]. In this paper, we review bio-inspired visual systems based on curved detector geometry and with neuromorphic preprocessing ability. We begin by introducing the fabrication, design features, and functions of curved image sensor-based bio-inspired visual systems. Then, we discuss visual systems with neuromorphic computing functions, focusing on photonic synapse and curved neuromorphic image sensor-based visual systems. Finally, we summarize the

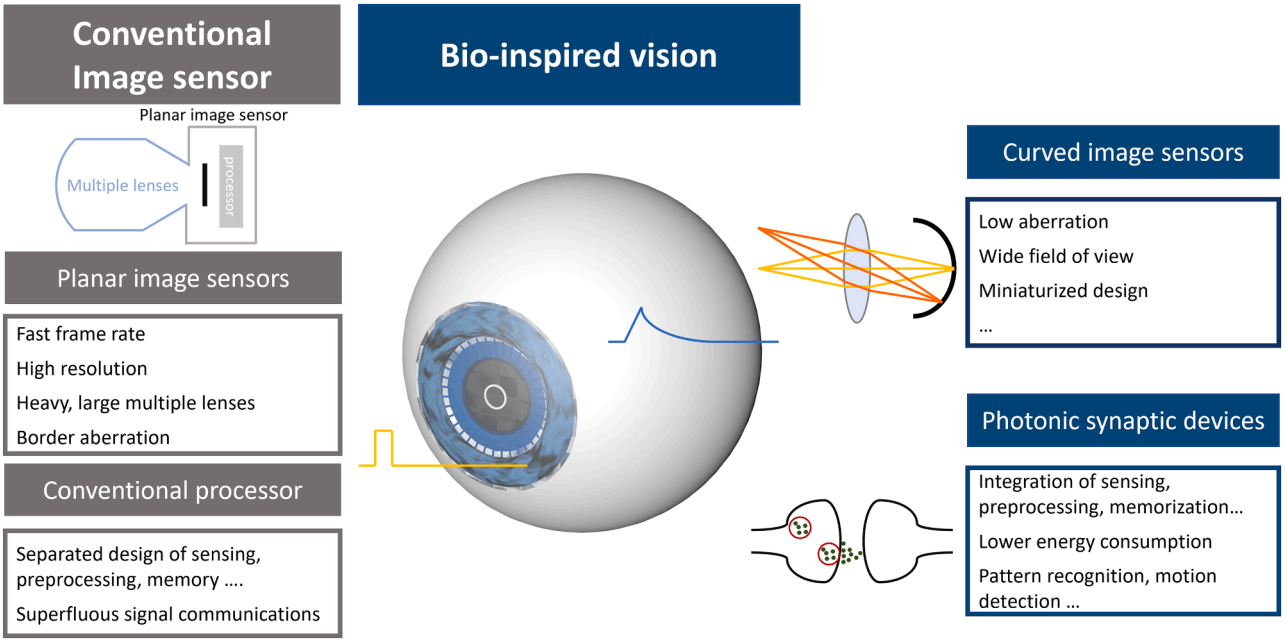

Fig. 1. Overview of conventional and bio-inspired visual systems.

development of bio-inspired visual systems and highlight some of the main challenges in related research areas.

Curved image sensor based bio-inspired visual systems

Inspired by biological eyes, visual systems with hemispherical detector geometry have been developed. Hemispherical artificial retinas offer low aberration imaging ability with simplified, miniaturized optical sub-systems. Additionally, bio-inspired optical sub-systems provide additional advantages such as a wide FoV, the ability to detect objects at different distances, and a large depth of field [23]. In this section, we will review the fabrication processes for curved image sensors, along with the designs and functions of typical bio-inspired visual systems.

Fabrication processes for curved image sensors

Curved detector geometry holds promise for advanced bio-inspired device designs, but the fabrication of curved image sensors presents a significant challenge. Conventional device patterning methods are unsuitable for non-planar substrates, necessitating the development of new methods. Two main approaches have been developed for fabricating curved image sensors: transferring planar patterns to curved geometry [10–19] and directly synthesizing materials on curved substrates [22–24]. However, these approaches have their own limitations and require specialized techniques.

In this section, we will summarize typical methods for fabricating curved image sensors. Firstly, we will overview pattern transferring methods, which include mechanical deforming, stretchable/compressible design, and foldable designs. Then, we will discuss curved-surface-compatible techniques, which are specifically designed for synthesizing materials on curved substrates. These methods have the potential to enable the development of new classes of bio-inspired visual systems with advanced imaging capabilities.

Mechanical deforming

Planar silicon-based image sensors, such as CMOS and CCD, are well-established with excellent resolution, dynamic range, sensitivity, and signal-to-noise-ratio. However, the high elastic stiffness, high strength, and low fracture toughness of single-crystal silicon used in CMOS/CCD sensor dies make controlled mechanical deformation challenging.

Recent progress has been made in mechanical deformation through the development of thinning processes. Dumas et al. fabricated a curved focal plane detector array with a radius of curvature of 80 mm based on a silicon-based device thinned to 50 μm [49]. The curved device showed no significant electrical performance degradation. Gregory et al. also demonstrated the reduction of overall thickness of devices to 200 μm based on a double-flush thinning process for back-illuminated CCDs. They achieved a yield of over 95 % for devices with a curvature up to 5.44 m [50]. Guenter et al. addressed the limitations of the conventional fixed edge deformation approach by developing a novel deforming process where the edges of the device can move freely. The edges of the device are subjected to greater compression, while the center is stretched relatively gently in the process. This approach resulted in a more stable deformation process, with a minimum radius of curvature of 16.7 mm. Their method takes advantage of the compressive strength of silicon, which significantly exceeds its tensile strength. This approach is shown in Fig. 2(a)–(c) and represents a significant advancement in the development of curved image sensors with advanced imaging

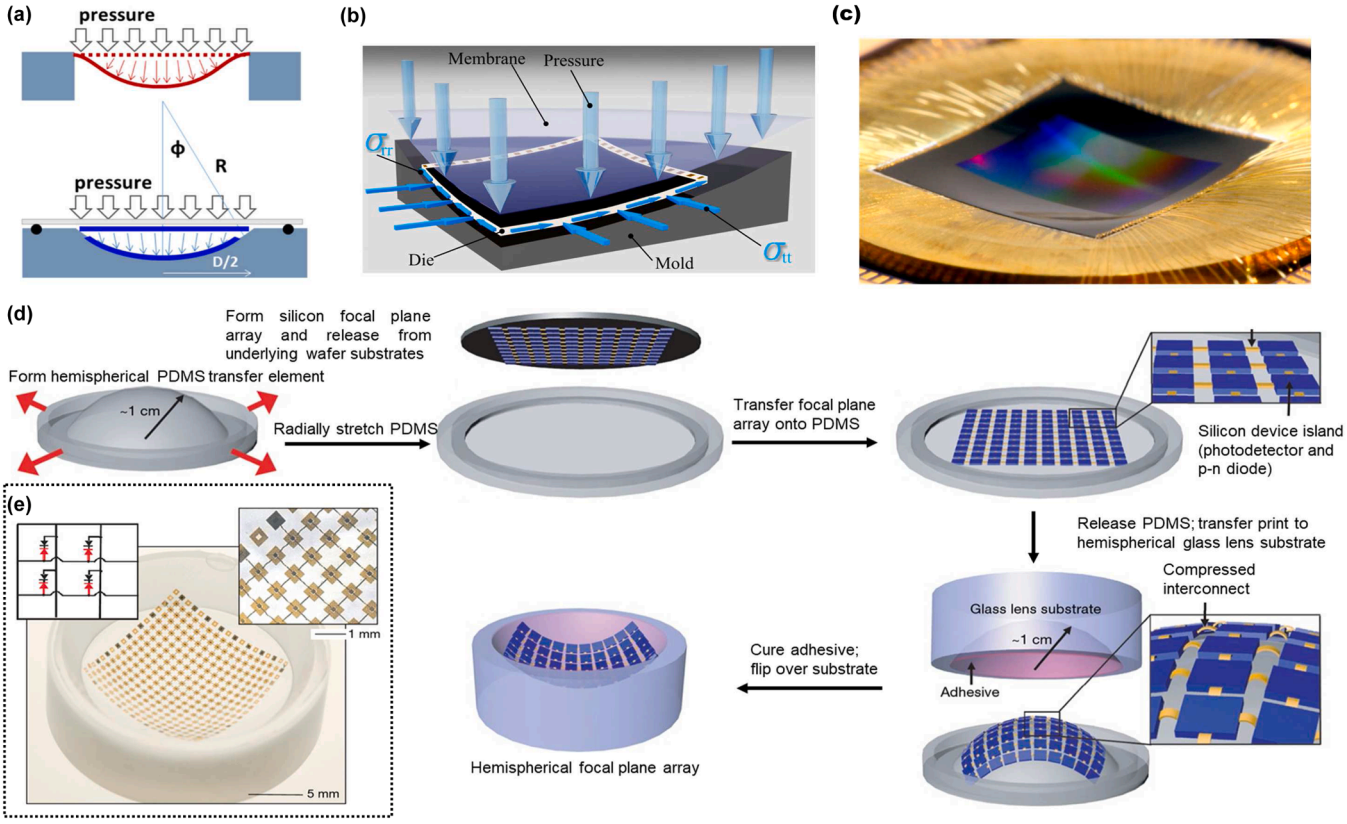

Fig. 2. Mechanical deforming process and Compressible island-bridge structure. (a) Comparison of conventional formation (upper, fixed edges) and pneumatic formation (lower, free edges). (b) Schematic diagram of the chip curving process. (c) A 18-megapixel CMOS curved image sensor bonded to a precise 18.74 mm curved mold surface. (a–c) Reproduced with permission [12]. Copyright 2017, Optical Society of America. (d, e) Compressible island-bridge structure enables curved image sensor. (d) Illustration of fabricating steps. (e) Photograph of a compressible focal plane array integrated on a hemispherical glass substrate (main frame), a portion of the array (upper right inset) and circuit diagram in a 2-by-2 section of the system (upper left inset). (d, e), Reproduced with permission [10]. Copyright 2008, Springer Nature.

capabilities [12].

The above fabricating approaches for curved image sensors are based on off-the-shelf devices with the addition of thinning and mechanical deforming steps, making them compatible with existing processes. Furthermore, the main parameters of the fabricated curved devices, particularly the pixel number, are similar to those of the latest planar image sensors. This technological route therefore has the greatest potential for industrialization. However, the mechanical properties of silicon, which is extensively used in image sensors, inherently limit its ability to be significantly curved due to its rigidity. This characteristic generally restricts the degree of curvature to less than 30° in most designs. Consequently, the subtended angle of these devices is limited, leading to a relatively minor enhancement in the FoV, usually less than 80°. There may also be concerns about the yield of the process and the stability of the devices, which were not well-stated in current studies. Therefore, further research is needed to overcome these challenges and to develop advanced fabrication techniques that enable the production of high-performance curved image sensors with the expanded FoV and improved stability. Such advancements will be critical for the development of bio-inspired visual systems with advanced imaging capabilities.

Stretchable/compressible design

The transformation from a 2D planar array to a 3D curved array inevitably involves the compression and stretching of the substrates and circuits. Polymers with high tensile strength and chemical stability, such as Polyimide (PI), are favored for flexible substrates and have been widely adopted [51–53]. In recent years, many ideas have emerged and developed for the design of stretchable/compressible circuits that provide excellent preservation of electrical performance. These circuits use various materials and patterning techniques, including serpentine interconnects, kirigami structures, and fractal geometries, to accommodate the deformation of the substrate without compromising the electrical properties of the circuits. These advances in stretchable/compressible circuit design have enabled the development of curved image sensors with advanced imaging capabilities, which can help to mimic the functionality of biological visual systems [54].

The island-bridge structure is a common strategy for stretchable electronic circuit design [55]. It consists of an array of rigid devices (islands), and stretchable or compressible interconnecting circuits (bridges). The mesh of islands and bridges exhibits excellent mechanical properties and can effectively protect the fragile active material without inducing undesirable changes in electrical properties. There are two typical approaches to implementing curved devices based on the island-bridge model. The first method for implementing curved devices based on the island-bridge model involves preparing the device on a curved substrate that is pre-stretched to a flat surface and detaching the bridges from the substrate. During the releasing of the substrate, the bridges absorb the majority of the stress [56]. Ko et al. demonstrated the application of the island-bridge structure in the development of a 16 × 16 hemispherical retina for an electronic eye based on this idea, as shown in Fig. 2(d) and (e) [10]. The other method for implementing curved devices based on the island-bridge model is to transfer the island-bridge structure from a planar flexible substrate into a curved shape, which requires the stretchability of the bridges, as shown in Fig. 3 (a). Jung et al. implemented a curvature-tunable image sensor using the island-bridge structure with serpentine interconnections (Fig. 3(b)–(d)) [9]. The use of finite element analysis has shown that with an overall biaxial strain of 12 %, the local strain was still less than 0.04 %, which is much lower than the fracture threshold. This demonstrates the potential for the development of stretchable electronic devices that can withstand significant deformation without damaging the fragile active material. In addition, fractal-inspired designs have been shown to be a feasible way to achieve extremely large stretchability and higher area filling ratios [57].

Despite their advantages, image sensors based on the island-bridge structure suffer from a low fill factor, which means that the active

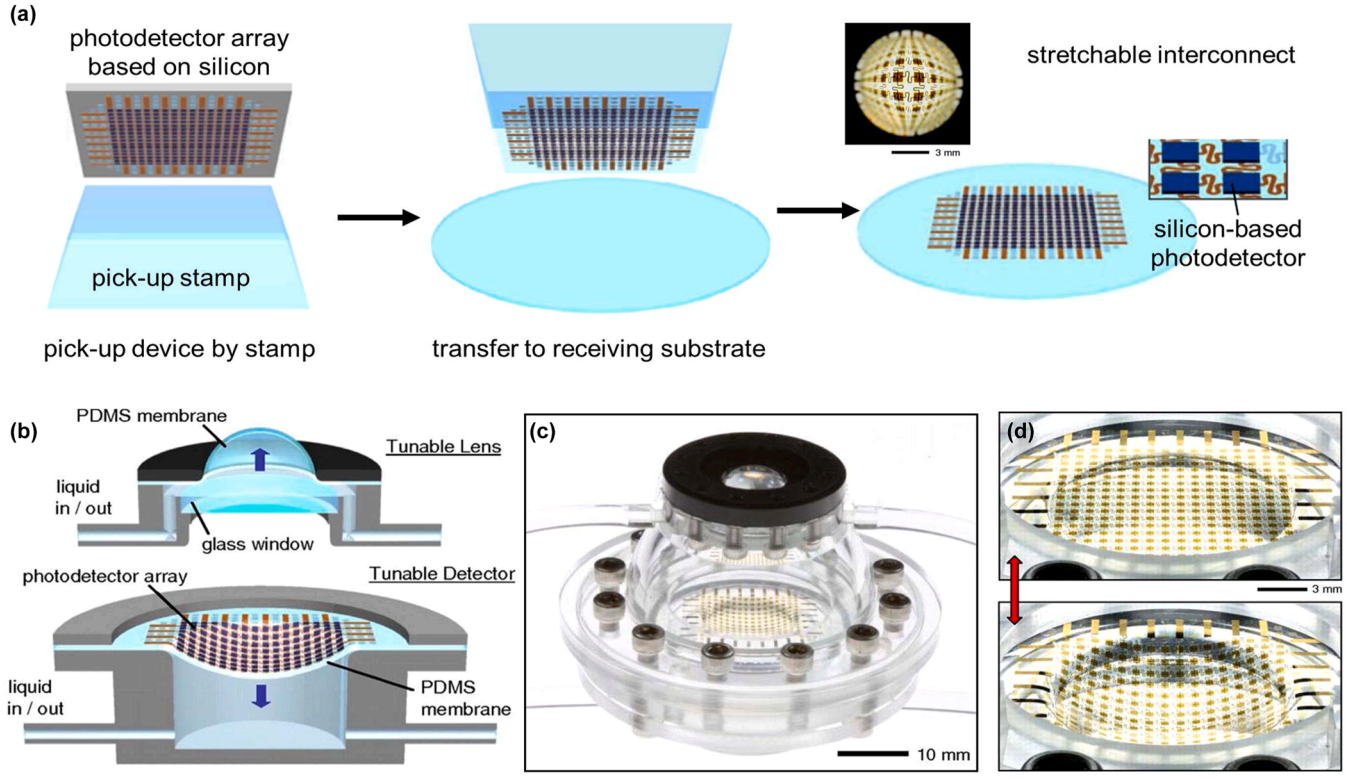

Fig. 3. Stretchable island-bridge structure enables curved image sensor. (a) Schematic illustration of fabricating steps. (b) Schematic illustration and (c) photograph of the integrated camera based on curved image sensor. (d) Optical image of a photodetector array from flat configuration (Upper) to hemispherical configuration (Lower). (a–d) Reproduced with permission [9]. Copyright 2011, National Academy of Sciences.

area is much smaller than the cell area. As a result, the resolution of the island-bridge structure is limited. While Ko et al. have addressed this issue by combining scanning (scans a modest range of angles, specifically between −2° to 2° for both the azimuthal angle in the plane normal to the optical axis and the polar angle measured from the optical axis, with increments of 0.4°), the integration of complex mechanics weakens the advantages of curved devices [10]. This trade-off between resolution and complexity is a key challenge in the development of curved electronic devices. To advance the field, new approaches are needed to increase the fill factor and resolution of curved devices while maintaining their mechanical properties. These advancements will enable the development of electronic devices with advanced functionalities, paving the way for new applications in the fields of robotics, biomedical devices, and wearable technology.

The kirigami design is another promising strategy for implementing stretchability, whereby a stable and controlled stretch is achieved by rotating pixels that are connected via identical hinges at the four corners. Rao et al. demonstrated the potential of this approach by developing a 32 × 32 image sensor with kirigami design that can fit complex curves [19]. The device has a fill factor of 78 % before stretching and maintains a fill factor of 46 % under 30 % biaxial stretching (Fig. 4(a)–(c)).

Foldable design

The foldable design approach is an inverse design from a 3D surface, which involves discretizing and reconstructing the 3D surface and unfolding it into a processable 2D circuit. Inspired by origami, Zhang et al. designed a folded hemispherical image sensor array using this approach [15]. The folded hemispherical image sensor array contains a total of 281 monocrystalline silicon photodetectors arranged in close proximity. Choi et al. demonstrated the potential of atomically thin MoS_2-graphene heterostructure in the development of a high-density curved image sensor array (Fig. 4(d)–(f)) [14]. Stress relief was achieved by truncating and folding the flexible planar array, which also prevented the emergence of wrinkles.

Lee et al. went beyond origami and achieved buckling-guided assembly to form different 3D geometries through precise mechanical design, as shown in Fig. 4(g) [58]. The results of the finite element analysis (Fig. 4(h)) indicate that this structure can effectively control the maximum strain. Building upon this approach, Xu et al. provided a detailed method for guiding buckling-guided assembly based on topology optimization, illustrating its effectiveness and applicability to the design of curved circuits [59].

While the foldable design approach is an attractive idea for enabling the development of stretchable and curved electronic devices, it still faces some challenges that need to be addressed. For example, the loss of pixels at joints and the lack of roundness of the curved surface can significantly impact the resolution and fill factor of the devices. Addressing these issues will be critical in advancing the field and enabling the development of electronic devices with advanced functionalities.

Curved nanowire array image sensor

Despite the advancements in the development of stretchable and curved electronic devices using planar semiconductor fabricating processes, such as photolithography, most of the methods described above

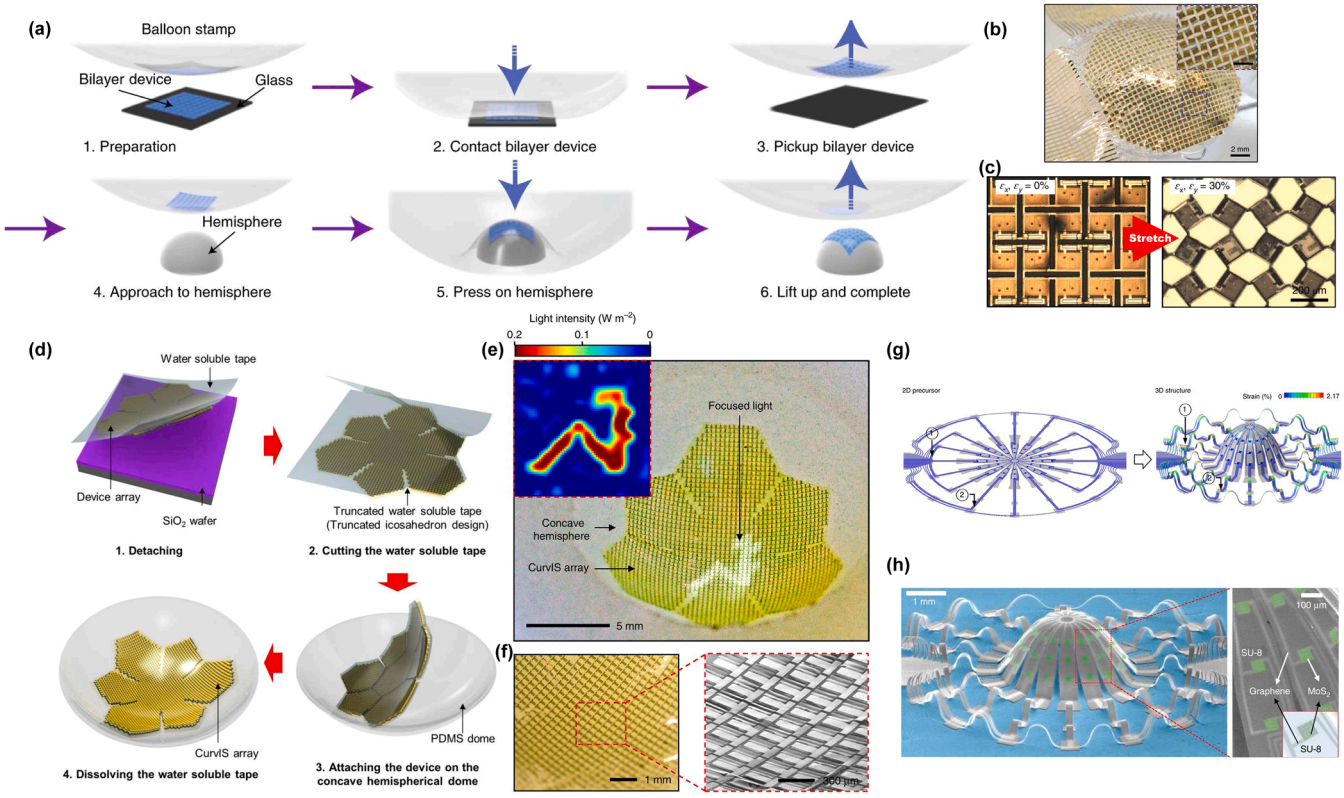

Fig. 4. Kirigami design and two foldable design, origami and buckling-guide assembly, to achieve curved image sensors. (a–c) A flexible kirigami-inspired photodetector array. (a) Schematic of the key fabricating steps (b) Photograph of the convex-shaped image sensor. (c) Photographs of the kirigami structure under different levels of biaxial stretch. (a–c) Reproduced with permission [19]. Copyright 2021, Springer Nature. (d–f) Origami inspired curved image sensor. (d) Illustration of fabricating steps. (e) Photograph of a hemispherical high-density photodetector array. Inset shows the image captured with this array. (f) Optical (left) and SEM (right) image of a part of the array. (d–f) Reproduced with permission [14]. Copyright 2017, Springer Nature. (g, h) A buckling-guided assembly structure enables curved image sensor. (g) Schematic illustration of fabricating steps. (g) Finite element analysis of the structures before (left) and after (right) compressive buckling, showing the distributions of principal strains. (h) SEM image of photodetectors on the 3D hemispherical structure. (g, h) Reproduced with permission [58]. Copyright 2018, Springer Nature.

still face limitations in achieving high-density integration. In this section, we will present techniques for direct device fabrication on curved substrates that are not constrained by conventional processes.

Self-assembled nanostructures, such as the porous aluminum membrane (PAM) [60–62] have attracted much attention in the development of electronic devices with advanced functionalities. Tavakoli et al. demonstrated the potential of template-assisted chemical vapor deposition (CVD) for the controlled and large-scale growth of perovskite nanowire array [63]. The method is universally applicable and can be used to grow a variety of perovskite nanowire arrays [64–68]. The nanowire arrays fabricated using perovskite materials are uniformly arranged perpendicular to the substrate with high quality and homogeneity. They not only retain the excellent optoelectronic properties of perovskite materials but also solve the critical problems of poor stability and integration difficulties. These advancements exhibit great potential for applications in high-performance three-dimensional optoelectronic devices [69–73]. In addition, the geometrical shape of the nanowire array can be adjusted according to specific requirements to regulate its optoelectronic properties, providing a wide range of possibilities for device design. Intriguingly, Gu et al. presented an electrochemical eye with a hemispherical retina made of a high-density array of nanowires that mimic the photoreceptors on a human retina (Fig. 5(a)) [22]. The device's design has a high degree of structural similarity to that of a human eye (Fig. 5(b)–(d)). Fig. 5(e) shows a cross-sectional image of the nanowire array. The size and number of pixels in the current device are determined and constrained by the diameter and number of liquid metal wires, but in principle, each nanowire can work independently as a photodetector. This indicates that this approach has great potential to achieve ultra-high-resolution imaging. Ding et al. further explored and demonstrated a biomimetic infrared sensor array with 625 pixels based on the hemispherical PAM and ionic thermoelectric materials (Fig. 5(f)) [24]. The precursor solution is filled into the PAM using the spin-coating method, and discrete nanowires are obtained after O_2 plasma etching. The backside electrodes are assembled by magnetic field-assisted alignment (Fig. 5(g)–(h)) with a minimum pitch of 550 μm.

In general, curved image sensors based on PAM can easily achieve high density integration of photo sensing units such as nanowires, have potential in developing diffraction limit imaging devices. Since PAM is directly fabricated on a hemispherical substrate, the devices are devoid of stress-related issues. However, it is still challenging to fabricate high density read out circuit on curve substrates that can realize high resolution imaging ability.

Other methods

Printing is a bottom-up preparation technique that has traditionally been performed on flat substrates. However, with the optimization of ink composition and advances in electrohydrodynamic, it is now possible to print directly onto curved surfaces. Printing metal electrodes [74,75], 3D antennas [76], graphene [77], and other materials on curved surfaces has been demonstrated. With further improvements in inkjet printing accuracy, it is likely that electronic devices will be printed directly onto curved substrates, enabling the efficient preparation of curved image sensors.

Table 1 summarizes some typical curved image sensors. While there are many promising approaches for designing curved image sensors, challenges such as maintaining high resolution and fill factor, as well as ensuring mechanical reliability, still need to be addressed. Nevertheless, the continued development of new materials, fabrication techniques, and design strategies is expected to enable the creation of highly functional and practical curved image sensors for a wide range of applications.

Structure and functions of bio-inspired visual systems

The majority of biological eyes can be divided into vertebrate eyes and compound eyes [78]. All detectors in a vertebrate eye share a single aperture and related optics that acquire images from the external world. The human eye is a vertebrate eye with a retina and a tunable optical system. Attractive design features of human eyes and other vertebrate eyes include a wide FoV, high resolution, and low aberration. In a compound eye, on the other hand, each ommatidium has its own aperture. Hence, a compound eye can achieve an ultra-wide FoV, low aberrations, high acuity to motion, and an infinite depth of field. The attractive structures of biological eyes have inspired a series of research on bio-inspired visual systems towards future visual prosthetic and machine vision applications, and beyond.

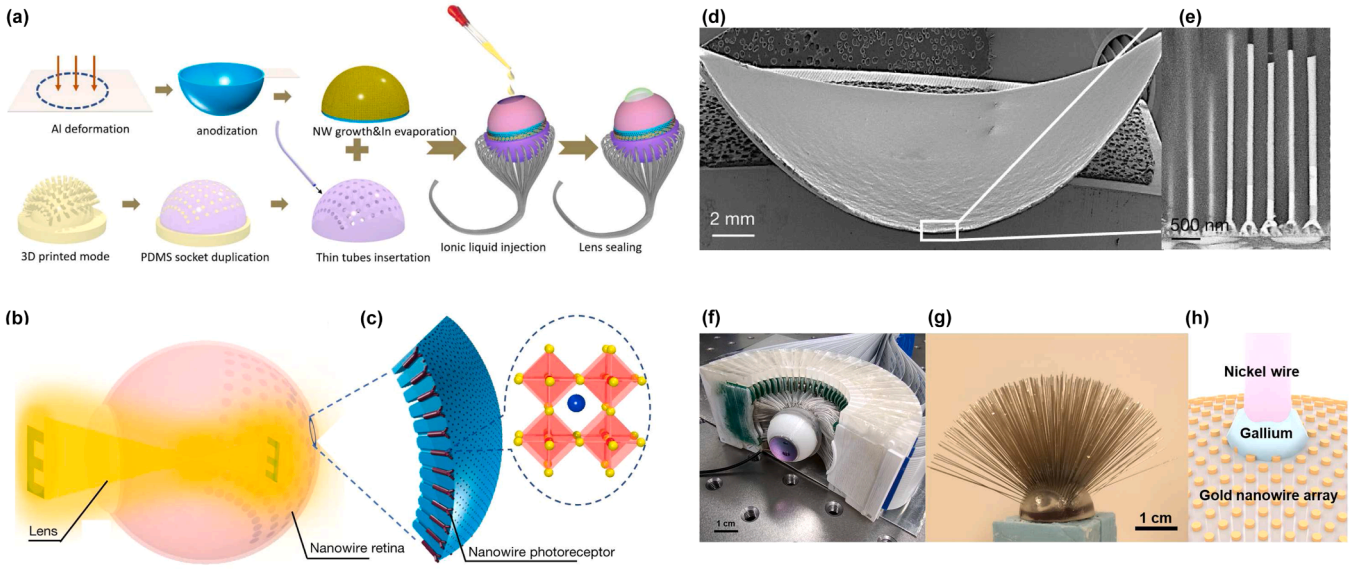

Fig. 5. Curved-surface-compatible techniques. (a–e) A biomimetic eye based on a hemispherical perovskite nanowire array. (a) Schematic of the fabricating steps. (b) Illustration of the working mechanism. (c) Illustration d, overall SEM image, and (e) cross-section SEM of perovskite nanowires in the hemispherical template. (a–e) Reproduced with permission [22]. Copyright 2020, Springer Nature. (f–h) Printing antennas on hemispherical surface. (f) Schematic illustration of the antennas on the 3D surface. (g) Photograph during the printing process. (h) Photograph of the completed antenna. (f, g) Reproduced with permission [24]. Copyright 2022, American Association for the Advancement of Science.

Table 1
Summary of typical curved image sensors.

Fabrication strategy		Device structure	Resolution (px)	Radius	Degree of curvature	FoV	Ref.
Mechanical deforming		Back-illuminated CCDs	4096 × 2048	5.44 m	~2°	70°	[50]
		Silicon CMOS image sensors	4880 × 3680	16.7 mm	26.7°	50°	[12]
Stretchable/ compressible designs	Compressible Island-bridge Structure	Silicon photodetector and *p-n* diode	16 × 16	~1 cm	80°	~80°	[10]
	Stretchable Island-bridge Structure	Silicon photodetector	16 × 16	11.4 mm	82°	53°	[9]
	Kirigami Design	Single-crystal Silicon photodetector	32 × 32	10 mm	~90°	~16°	[19]
Foldable designs	Origami Design	MoS_2-graphene heterostructure	281	2.27 mm	~180°	~13°	[14]
	Buckling-guided Assembly	MoS_2-graphene	48	1.26 mm	~180°	N/A	[58]
Curved-surface-compatible techniques	Template-assistant Growth	$FAPbI_3$ nanowires	10 × 10	10 mm	130°	100°	[22]
		i-TE nanowires	25 × 25	10 mm	150°	135°	[24]
		$CsPbI_3$ nanowires	252	10 mm	160°	140°	[23]

Visual systems inspired by human eye

In recent years, there has been significant research into developing visual systems that are inspired by the human eye. The human eye has a roughly spherical geometry, which allows for low-aberration imaging with few-component imaging optics. It also has an ultra-wide FoV of 150° and a high photoreceptor cell density of $>10^5$ mm^{-2}, which supports high-resolution imaging ability. A typical human-eye-inspired visual system contains a single-lens-based optical system and a concave image sensor.

Fig. 6(a)–(c) shows a human eye inspired hemispherical electronic eye camera based on compressible silicon optoelectronics reported by Ko et al. [10]. Fig. 6(a) shows a photo of such a system, integrated by a hemispherical image sensor and a single lens. The hemispherical detector geometry is supported by a compressible and stretchable device design. This artificial retina has 16 × 16 pixels, with each pixel having a footprint of 500 × 500 μm^2 in area, 1.2 μm thick silicon layer covered

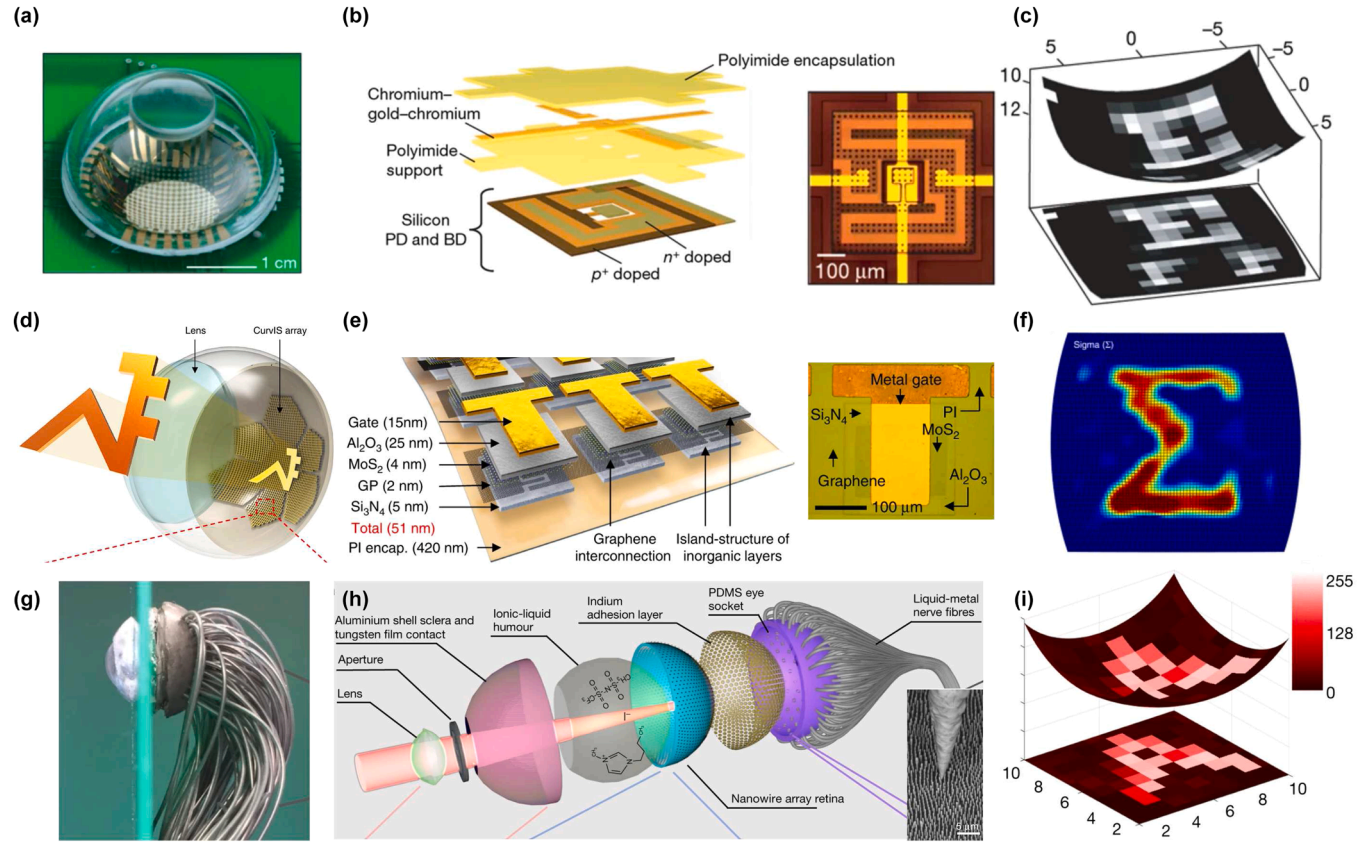

Fig. 6. Bio-inspired visual systems based on single fixed lens. (a) Photograph of a human eye inspired hemispherical electronic eye camera after integration with a transparent (for ease of viewing) hemispherical cap with a simple, single-component imaging lens (top). (b) exploded schematic of the layout of the silicon, metal and polymer associated with a single unit cell in the array. The blocking diode (BD) is in the center of the cell; the photodetector (PD) is in a serpentine geometry around the BD. (c) Greyscale images of the first two rows in an eye chart acquired using a hemispherical camera with a 16-by-16 pixel array, as displayed on a hemispherical surface matching the detector surface (top) and projected onto a plane (bottom). (a–c) Reproduced with permission [10]. Copyright 2008, Springer Nature. (d) Schematic illustration of the human eye inspired high-density curved image sensor array based on the MoS_2-graphene heterostructure. (e) Schematic illustration of the device design. Inset shows an optical microscope image of a single phototransistor. f, Sigma-shaped image captured by the curved image sensor array. (d–f) Reproduced with permission [14]. Copyright 2017, Springer Nature. (g) Side view and (h) exploded view of the biomimetic eye (electrochemical eye, EC-EYE). Inserting figure of h shows the image of the Ni microneedle contact to the nanowire array. (i) Back-view photo of an EC-EYE mounted on a printed circuit board. (g, h), Reproduced with permission [22]. Copyright 2020, Springer Nature.

with a 560 × 560 μm^2 in area, 1–1.5 μm thick polyimide capping layer. Adjacent pixels are connected by a 360 μm long, 50 μm wide, 156 μm thick layer of metal on a 360 μm long, 110 μm wide, 1–1.5 μm thick polyimide layer. To absorb bending-induced strains, interconnect layers are used, and the rigid silicon image sensor can be bent to a hemispherical shape. The interconnects consist of thin layers of patterned metal (chromium and gold) on thin layers of polyimide. The detailed structure of one photo sensing unit is shown in Fig. 6(b). Each photo sensing unit contains a silicon photodiode and a current-blocking p-n junction diode to suppress crosstalk. Specifically, the current-blocking diodes are covered by a metal layer to avoid unwanted photo response. Fig. 6(c) shows the grayscale image of the first two rows in an eye chart acquired by such a visual system. Furthermore, higher-resolution images can be acquired by such a system with scanning.

The interconnect layers in this system allow for the fabrication of curved image sensors, although they also take up space and limit the resolution. To fabricate a bionic eye with higher resolution, higher density designs based on thinner and softer materials provide an alternative. Choi et al. reported a human-eye-inspired visual system based on a MoS_2-graphene curved image sensor array [14]. Fig. 6(d) shows the schematic of such a system. To further reduce the bending strains, the artificial retina has a distinctive truncated icosahedron design. The image is also acquired by a single fixed lens. Fig. 6(e) shows the detailed structure of each pixel. Each pixel consists of a 51 nm thick photo sensing unit supported by 420 nm polyimide (PI) encapsulations. The absorbing layer and interconnection layer are MoS_2 (six layers) and graphene (four layers), respectively. Fig. 6(f) shows the image of a Sigma-shape detected by the artificial visual system. Notably, because MoS_2 has a relatively wider bandgap, this system can avoid infrared (IR) absorption-related problems that occur in conventional silicon image sensor-based image systems.

Another approach to developing a human eye-inspired visual system is to use a nanowire array-based hemispherical retina, as reported by our group [22]. Fig. 6(g) shows the photo of it, and the detailed design is shown in Fig. 6(h). This system uses a hemispherical porous aluminum membrane instead of bending a planar pattern to a hemispherical shape, so there are no bending strain-related problems and a potential for high resolution. The pitch between nanowires is ~500 nm, corresponding to a density of 4.6 × 10^8 cm^{-2}, even higher than the density of photo receptor cells in human retina. Each nanowire has a strong enough photo response to be measured, thanks to the excellent optoelectronic performance of perovskite ($FAPbI_3$). The nanowires are effectively isolated from each other by the porous aluminum membrane, which efficiently suppresses crosstalk. Optical elements, including a fixed lens and an iris, help to acquire images from the external environment. By using a hemispherical retina geometry, the system has a wide FoV of 100.1°, significantly wider than a planar image sensor-based system (69.8°).

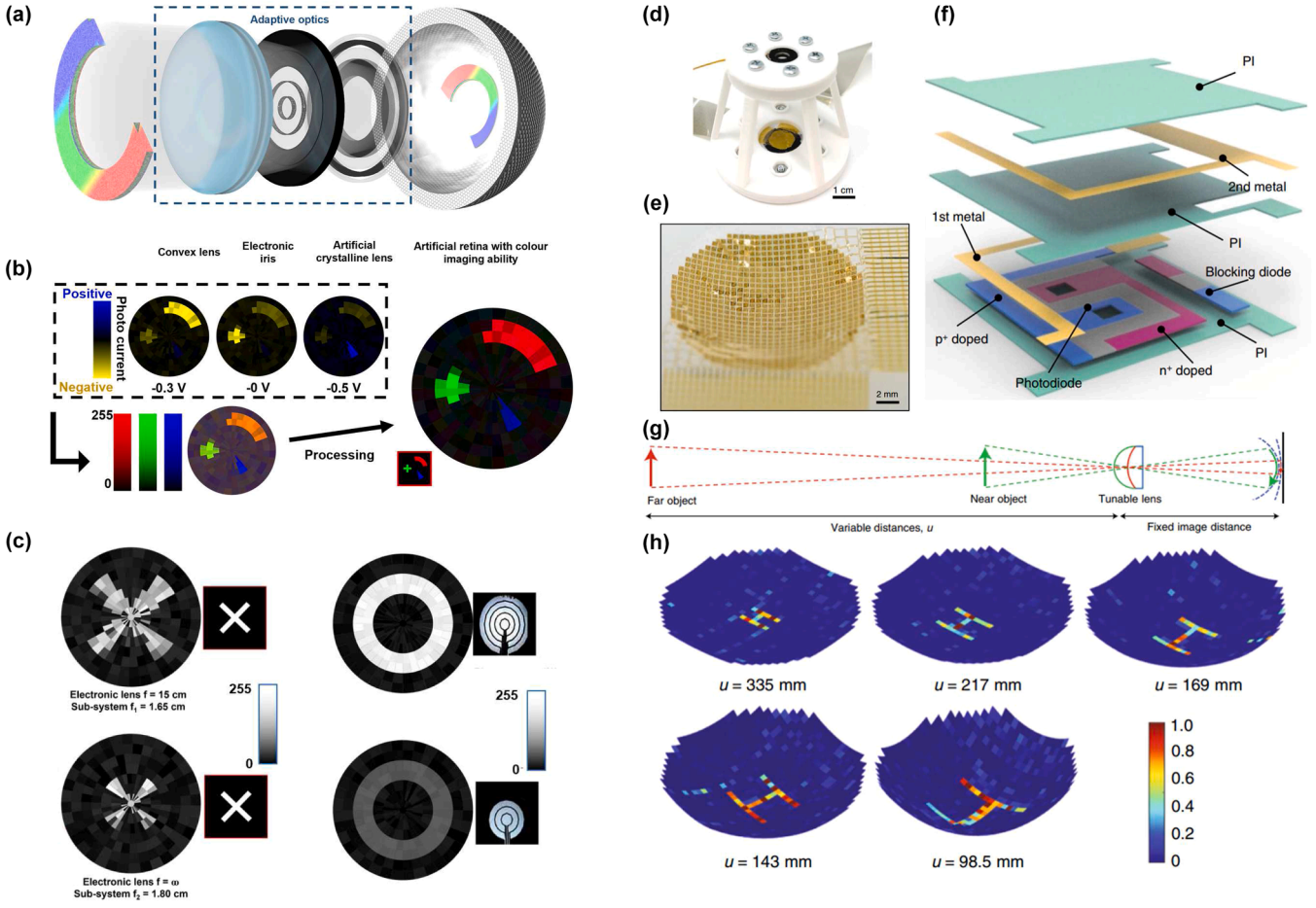

Fig. 7. Bio-inspired visual systems based on tunable optics. (a) The schematic of the bionic eye system with adaptive optics. (b) Images of different distance objects acquired by the bionic eye with different focal lengths. (c) Images of the same object with different iris conditions. (d) Demonstration of color pattern reconstruction. (a–d) Reproduced with permission [23]. Copyright 2023, Springer Nature. (e) Optical image of the assembled Human-eyeball-inspired adaptive imager. (f) Schematic of a single-crystal Si-based optoelectronic pixel in an exploded view, each pixel consists of a photodiode and a blocking diode. (g) Optical image of the concave-shaped imager. (h) Schematic of the adaptive imager with tunable focusing power to see objects at variable distances. The image distance is fixed, while the curvatures of both the lens and focal planes are variable. And imaging results acquired by the adaptive imager for objects at different distances. The series of images were rendered on the corresponding curvy planes. (e–h) Reproduced with permission [19]. Copyright 2021, Springer Nature.

However, the resolution is still limited by the backside wire bonding strategy. Liquid-metal nerve fibers have a diameter of ~700 μm and a pitch of ~1.6 mm, which can hardly achieve high resolution. To optimize the backside electrode array, a magnetic field-aligned nickel needle contact is demonstrated, shown in the inserted figure of Fig. 6(h). Each nickel needle has a diameter of ~50 μm, and the diameter at the top of such a needle is less than 1 μm, so that each nickel needle can theoretically contact with 3 nanowires. Fig. 6(i) shows the image of the shape "A" acquired by the biomimetic eye.

Beyond a fixed optical system, a human eye has evolved tunable optics, including a crystalline lens and an iris, that enable excellent adaptivity. The crystalline lens can modify its focal length by changing its thickness so that we can see objects clearly at different distances. The iris can change the shape of the pupil and enable a human eye to have a large dynamic range. Inspired by such a structure, our group fabricated another bionic eye device with tunable optics. The schematic of the device is shown in Fig. 7(a) [23]. Apart from the fixed convex lens, a tunable lens and iris are integrated into the system. Both optics are based on liquid crystal, which has a thin thickness (down to <1 mm) and can be switched quickly (<16 ms). By switching the artificial crystalline lens, the focal lengths of the system can be changed so that objects from different distances can be imaged clearly (Fig. 7(b)). The artificial iris can change its ``pupil'' to enhance the dynamic range of the bionic eye. Fig. 7(c) shows two images detected by the device with different iris conditions. Moreover, we also achieved full-color imaging ability on such a hemispherical device. By changing external bias, the color selectivity of each pixel can be tuned so that RGB-based color information can be acquired after three measurements. Fig. 7(d) shows the color pattern reconstruction of the device.

The changing of focal length can also change the Petzval field curvature, which may cause a mismatch with the image sensor. Therefore, the fabrication of a curved image sensor with a changeable shape is desired. Rao et al. reported a tunable lens-based visual system that integrates a curvy, shape-adaptive image sensor with kirigami design [19]. Fig. 7(e) shows the photo of the visual system. Fig. 7(f) shows the schematic of a single-pixel structure. Each sensing unit has a photodiode for light sensing and a blocking diode to avoid crosstalk. Fig. 7(g) shows the photo of the curved retina. The kirigami design provides a promising approach to fabricate a high-density curved image sensor with rigid materials. The inserted figure shows the photo of a single pixel. Fig. 7(h) shows the imaging principle and a shape "H" detected by the system with different focal length conditions. When the thickness of the tunable lens changed, the curvature of the focal plane also changed so that a fixed curved image sensor cannot always match the focal plane. To further reduce aberration, the visual system can tune the shape of the image sensor according to the thickness of the tunable lens. With a longer focal lens and a longer object distance, the image sensor should be flatter to match the focal plane. And for near objects viewed with a shorter focal length, the curvature of the image sensor needs to be higher.

In summary, human eye-inspired visual systems contain single-lens-based optical subsystems and curved artificial retinas, which provide promising methods to develop low-aberration visual systems. Simplified optical systems can reduce the size and weight of visual systems and further expand their applications in visual prostheses, machine vision, and beyond.

Visual systems inspired by other biological eyes

Apart from human eye, animals developed their unique eye structure for different environment during evolution. And those eyes also provide inspirations in artificial visual system design.

Some aquatic animals, such as fish, have eyes with a wide FoV. Inspired by aquatic vision, Kim et al. demonstrated a visual system based on a monocentric lens and a hemispherical silicon nanorod photodiode array (h-SiNR-PDA) [17]. Fig. 8(a) shows the structure of the optical subsystem. The monocentric lens has a spherical and symmetric shape. It is assembled with one half-ball BK7 lens (radius $R_{in} = 2$ mm, refractive index $n_{in} = 1.52$) and shell SF16 lens (radius $R_{out} = 4.1$ mm, refractive index $n_{out} = 1.65$) on both sides of the aperture, which is a transparent optical adhesive (NOA 61). The outer shell has a larger refractive index to achieve a shorter focal point radius. Fig. 8(b) shows the schematic of the aquatic vision-inspired system. The shape of h-SiNR-PDA matches with the hemispherical focal plane of the monocentric lens, thus light from wide angular directions can be effectively focused and detected. Such a system has a wide FoV of 120°. Besides, the nanorod structure exhibits a light trapping effect arising from diffraction that can enhance the photo absorption and optimize signal to noise ratio. Fig. 8(c) shows the photograph of the assembled aquatic-vision-inspired camera module. The artificial retina is a mesh-shaped 23 × 23 hexagonal pixel array. The silicon nanorods have a height of 220 nm, a diameter of 200 nm, and a pitch of 520 nm. A passivation layer of Al_2O_3 was applied to suppress

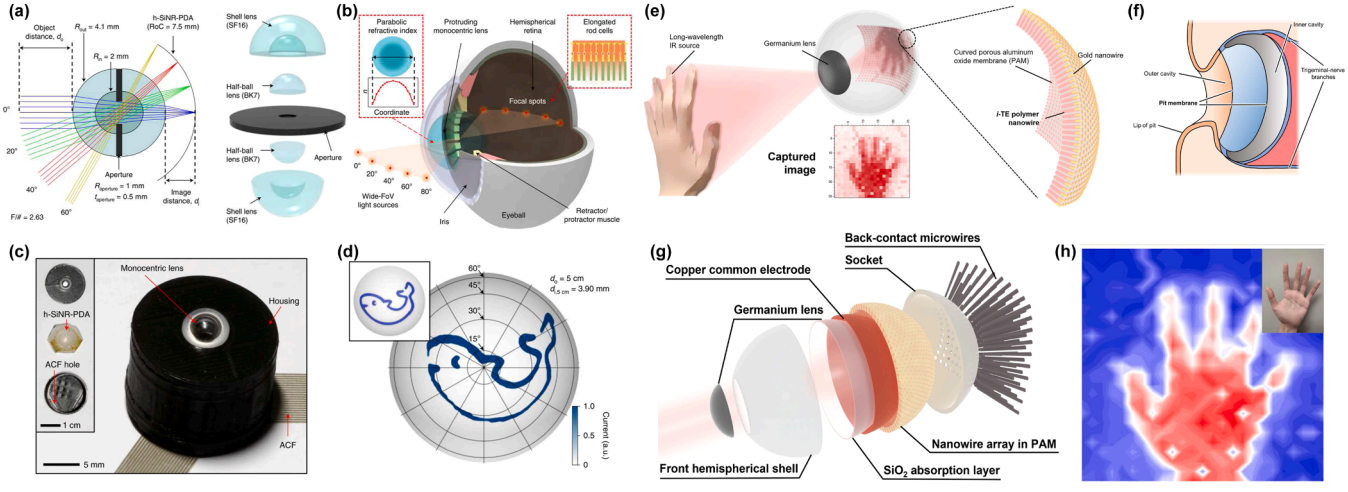

Fig. 8. Other single eyes inspired biomimetic visual systems. (a) Ray-tracing simulation of the aquatic-vision-inspired camera. RoC, radius of curvature. And exploded schematic of the monocentric lens. (b) Schematic of the aquatic eye with its key features. Left inset: parabolic RI profile of the protruding monocentric lens. Right inset: highly sensitive elongated rod cells in the hemispherical retina. (c) Photograph of the assembled aquatic-vision-inspired camera module. Inset: its disassembled form. (d) Panoramic imaging demonstration (FoV = = 120°). Inset: the original object image. (a–d) Reproduced with permission [17]. Copyright 2020, Springer Nature. (e) Schematic of the pit organ from a cross-sectional view. (f) Exploded schematic of PIT device. (g) Schematic of the working mechanism of PIT device. (h) Captured images of human hand at room temperature. (e–h), Reproduced with permission [24]. Copyright 2022, American Association for the Advancement of Science.

the surface leakage current. Each pixel contains a silicon nanorod photodiode and a blocking diode. Fig. 8(d) shows a fish-shaped image captured by the aquatic vision-inspired camera.

The non-visible light detection and imaging ability of some animals can be replicated in biomimetic visual systems for special applications. Specifically, infrared (IR) imaging and thermography are highly desired in applications including night vision, thermal mapping, and medical imaging. The pit organ (Fig. 8(e)) based IR imaging strongly supports pit vipers in hunting warm-blooded small animals. Inspired by such a structure, our group reported an artificial pit organ based on ionic thermoelectric polymer nanowire arrays [24]. The device structure is shown in Fig. 8(f). The germanium lens serves to focus IR light and absorb visible light, giving rise to a visible-blind IR imaging ability. The SiO_2 absorption layer can absorb IR light and generate a temperature difference between the two sides of the nanowire array. The ionic thermoelectric polymer nanowire arrays convert the temperature gradient to a voltage signal based on the thermoelectric effect. The imaging process schematic and the gesture detection result are shown in Fig. 8(g) and (h), respectively. Because of the efficient conversion of IR signal to electric voltage via the thermoelectric effect, the device can work without an external power source. The reduction in energy consumption also leads to less heat production. Therefore, the device has an uncooled and self-powered feature. It is worth noting that the device has 625 pixels and an ultrawide FoV of up to 135°.

Compound eyes can be found in arthropods such as insects. Compared to vertebrate eyes, compound eyes always have a much wider FoV, infinite depth of field, and high acuity to motion. Thus, compound eye-like visual systems have great potential in monitoring and other applications. Inspired by arthropod eyes, Song et al. developed a compound eye camera with nearly full hemispherical shapes (~160°) [13]. As shown in Fig. 9(a), the surface of the convex image sensor is covered with dense artificial ommatidia. The number of ommatidia (180) is comparable to the eyes of fire ants and bark beetles. Fig. 9(b) shows the cross-section schematic of ommatidia. The elastomeric micro-lens array (made of poly(dimethylsiloxane), PDMS, with a refractive index of $n \approx 1.43$) serves to focus light and define the overall mechanics. Each micro-lens (with a radius of curvature of $r \approx 400$ μm) is on a matching cylindrical supporting post (of height $h \approx 400$ μm) supported by a ~550 μm thick base membrane. Each micro-lens can only focus light within the acceptance angle ($\Delta\phi = 9.7°$), so that the shape of the objects can be acquired by the combination of micro-lenses. Fig. 9(c) shows the schematic and photo of artificial ommatidia. Underneath each micro-lens, there is a photo-sensing unit combined with a photodiode and a blocking diode. The active area of a silicon photodiode is d2 ≈ 160 μm × 160 μm. The inter-ommatidial angle ($\Delta\Phi = 11.0°$) defines the angular object space detected by each ommatidium. For $\Delta\varphi < \Delta\Phi$, there is no overlap field between ommatidia. Fig. 9(d) shows the shape of a fly detected by the arthropod eye-inspired visual system.

Nevertheless, Lee et al. developed an amphibious visual system inspired by the eye structure of a fiddler crab [18]. The spherical device can break the limitation of hemispherical geometry and reach >180°FoV. The device is shown in Fig. 9(e). Pixels are distributed over almost the entire spherical surface to reach an ultra-wide FoV (horizontally 300° and vertically 160°). At the pixel level, Fig. 9(f) shows the optical structure of a fiddler crab, including a graded-index corneal lens (GCL), crystalline cone (CC), and screening pigment (SP). Based on such an ommatidium with a gradient refractive index, light can be efficiently focused on the photoreceptor in both air and underwater environments. Thus, a fiddler crab can have clear amphibious vision. The amphibious visual system also integrates micro-lenses with a gradient refractive index (Fig. 9(g)). Fig. 9(h) and (i) show the schematic and imaging result of the amphibious imaging system.

In all, evolution has created distinctive eye structures with extraordinary abilities that strongly support the behavior of humans and other animals. Inspired by biological eyes, bio-inspired visual systems are developed towards miniaturization, lightweight, low aberration, and high resolution. The core technology is the hemispherical device geometry fabrication methods. Promising approaches have been

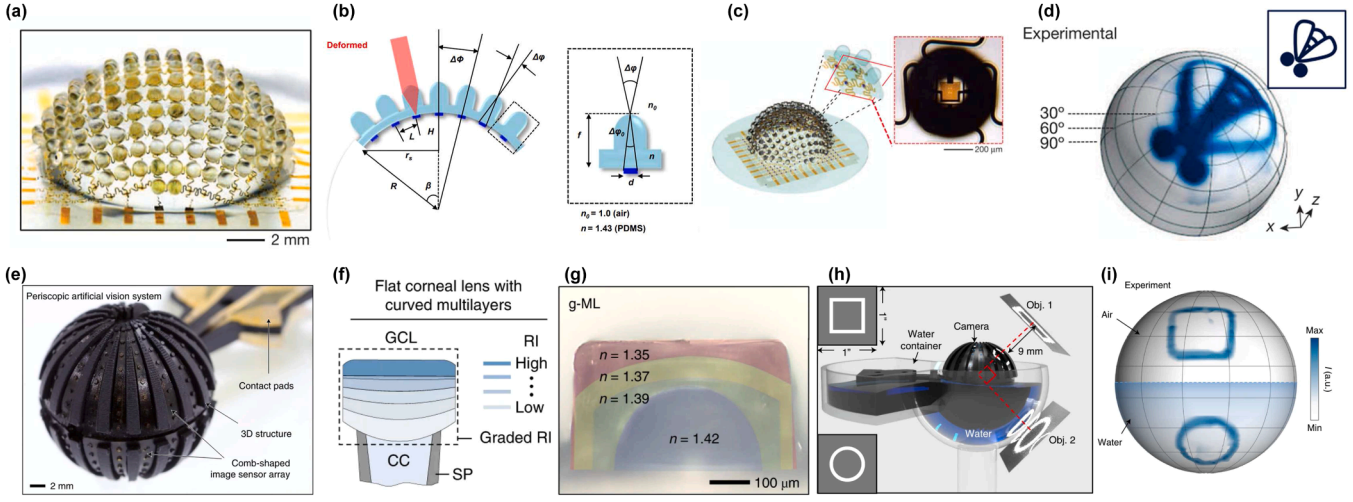

Fig. 9. Compound eyes inspired biomimetic visual systems. (a) Image of the arthropod eye inspired system after hemispherical deformation. (b) A cross-sectional illustration of the micro lens array that highlights key parameters: the acceptance angle (DQ) for each ommatidium, the inter-ommatidial angle (DW), the radius of curvature of the entire device (R) and of an individual micro lens (r), the height of a cylindrical supporting post (h), the thickness of the base membrane (t), and the diameter of the active area of a photodiode (d). (c) Illustrations of an array of elastomeric micro lenses and supporting posts joined by a base membrane and a corresponding collection of silicon photodiodes and blocking diodes interconnected by filamentary serpentine wires and configured for matrix addressing. Bonding these two elements and elastically deforming them ('combine, stretch') into a hemispherical shape creates the digital imaging component of an apposition compound eye camera. (d) An exploded view off the adjacent unit cells appears in the inset. (a–d) Reproduced with permission [13]. Copyright 2013, Springer Nature. (e) Photograph of artificial vision. Photodetectors and microlenses are integrated on the spherical 3D structure. The dots on the ellipsoid show the locations of the microlenses and photodetectors. (f) Comparison of the biological (left) and artificial (right) ommatidium. (g) Magnified cross-sectional view of g-ML. The colourized layers show the graded interlayer structure and flat surface of g-ML. (h) Experimental setup for the amphibious imaging demonstration. Two objects (Obj. 1 and Obj. 2) located at a distance of 9 mm were projected onto the artificial vision system with an angular difference of 90°. A transparent water container was filled halfway to create the amphibious environment. (i) Image obtained by artificial vision in an amphibious (air–water) environment. (e–i) Reproduced with permission [18]. Copyright 2022, Springer Nature.

developed and reviewed in previous discussions. However, there are still challenges for commercial applications. One major challenge is the resolution. State-of-the-art curved image sensors have pixel pitches over 100 μm, which are much larger than those of commercial planar image sensors (typically <10 μm). Moreover, because the hemispherical color filter array is hard to fabricate, most bio-inspired visual systems can only image grayscale patterns. Therefore, high-resolution, color image sensors in hemispherical shape, and related visual systems are desired.

Performance parameters for curved image sensors

In preceding sections, we have outlined the potential of innovative bionic eyes based on curved image sensors. These sensors show immense promise in a wide range of artificial vision applications. Crafted for superior imaging capabilities, the performance of a curved image sensor is typically evaluated based on parameters such as the level of curvature, resolution, and FoV.

The degree of curvature is a key parameter defining the geometry of a curved image sensor. It significantly influences the sensor's ability to capture images that closely replicate human visual perception, thus facilitating high-quality imaging with fewer optical elements. A greater degree of curvature can mitigate the distortions commonly associated with flat sensors, leading to more accurate and realistic images. The curvature level can be characterized by the degree of curvature and the angle of curvature. Presently, the development of hemispherical image sensors, featuring near 180° curvature angles, shows great promise for low-aberration imaging applications.

Resolution indicates the level of detail an image sensor can capture. Image sensors with higher resolution can detect and register more intricate details in a scene, leading to clearer, sharper, and more detailed images. The resolution of an image sensor is typically measured by its pixel count. The greater the number of pixels, the higher the potential for capturing detailed imagery.

The FoV of an image sensor plays a pivotal role in defining the range of the observable world that the sensor can capture in a single frame. A wider FoV allows the device to encompass a larger scene within a single image, providing a broader perspective of the environment.

A comprehensive comparison of various curved image sensors is presented in Table 1. This table brings together the primary performance parameters for each sensor, offering a side-by-side analysis that assists in understanding their capabilities and characteristics.

Role of photonic synapses in neuromorphic computing

Additionally, another challenge in bio-inspired visual systems is the integration of the optical and electronic components. In biological eyes, the photoreceptor cells and neural processing occur in close proximity, allowing for efficient information transfer [26,79]. Since Mead firstly mimic biological neuron network in the 1980s, neuromorphic hardware has shown potential in various applications [44]. To emulate the integration of visual sensing, preprocessing, information relay, processing and memorization, neuromorphic visual systems have come to the fore. Such systems provide potential in multifarious applications in visual prosthetics and artificially intelligent robotics [28]. Hardware artificial neuromorphic visual systems are explicitly designed to mimic the human visual system, and they generally consist of two layers. The first layer is primarily composed of an artificial photonic synapse that senses the visual information and performs some initial image pre-processing and memorization. The second layer typically consists of electronic artificial synapses made of non-volatile memory technologies like resistive random access memory (RRAM), phase change random access memory (PCRAM), and magneto resistive random access memory (MRAM). These synapses can perform advanced processing and computing tasks like recognition and classification, and they can store the perceived visual information after being trained with machine learning algorithms [26,28,79]. In this section, we will explore the reported details of photonic synapses, including the different device structures and materials used, synaptic performance parameters, and their potential applicability in artificially intelligent visual systems.

Typical materials for photonic synapses

Traditionally, photonic synapses have been reported in two forms: two-terminal memristors and three-terminal phototransistors. Two-terminal devices have successfully emulated synaptic functions like STP and LTP, with additional advantages of large-scale integration in high-density crossbar array architecture [35]. On the other hand, the phototransistor architecture can also effectively emulate STP/LTP synaptic traits, with the added benefit of simultaneous signal relay and learning [40]. Various material systems have been utilized to realize both two-terminal and three-terminal photonic synapses, including oxides and halide perovskites. We will provide a detailed discussion of these materials below.

Traditional oxide and sulphide based photonic synapses

A plethora of metal oxides with excellent photoconduction and facile, easy fabrication have been vigorously utilized as photonic synapses in recent years [27,41,42]. Two-terminal oxide-based devices typically use the oxide material as a sandwiching layer between two electrode contacts or as heterojunctions that involve photoconduction attributed to electron tunneling or ionic diffusion. Kumar et al. reported on a two-terminal synaptic device based on zinc oxide (ZnO), with the active layer sandwiched between indium oxide (In_2O_3) and fluorine doped tin oxide (FTO) contacts (Fig. 10(a)–(g)) [30]. The device operates on the principle of charge trapping and de-trapping under variable bias at the ZnO/In_2O_3 interface, and thus exhibits photoconduction (Fig. 10(b)). Under UV illumination, the device exhibits subsequent memorization upon switching off the light and returns to its initial conduction state with negative electrical bias. Similar to the human visual system, the devices show enhanced photocurrent with increased intensity of the stimulating light (Fig. 10(c)), paired pulse facilitation (PPF) as shown in Fig. 10(d)–(f), and long-term synaptic learning in the form of optical potentiation and electrical depression (Fig. 10(g)). In addition to the simple thin-film architecture, ZnO has also been utilized to form photonic synapses using horizontally laid nanowires or vertically assembled nanorods [33,40]. Vertically assembled nanorod devices have the added advantage of high-density integration in crossbar array architectures and scaled-down device size. Wang et al. reported on a three-terminal photoelectric synaptic transistor utilizing a molybdenum disulfide (MoS_2)/perylene tetracarboxylic dianhydride (PTCDA) heterojunction, as shown in Fig. 10(h)–(k) [38]. In order to mimic the neurotransmitter release in biological synapses, electron exchange in the heterojunction, in conjunction with the photogating effect (Fig. 10(i)), leads to the realization of STP and LTP behaviors. Fig. 10j shows the PPF characteristics of such a device and the transformation from STP to LTP mode of learning with changing gate voltage. As the number of laser pulses increases, the synaptic connectivity of the device becomes stronger, as exhibited by synaptic number-dependent plasticity (SNDP) based LTP learning in Fig. 10(k).

Perovskite based photonic synapses

Due to their tunable bandgap, long charge diffusion length, high absorption coefficient, and high color purity, halide perovskites (HPs) have garnered tremendous scientific interest in the field of optoelectronics [34,36,80–84]. In addition to their excellent optical properties, HPs also possess abundant ion migration pathways, hysteresis, and defect states, which facilitate trapping and de-trapping of photo-generated charges. As a result, HPs have recently been used extensively in the development of photonic synapses [29,43]. Ma et al. reported on a two-terminal photo-synaptic device based on cesium lead bromide ($CsPbBr_3$) nanoplates, as shown in Fig. 11(a) [31]. The cross-sectional high-resolution transmission electron microscope

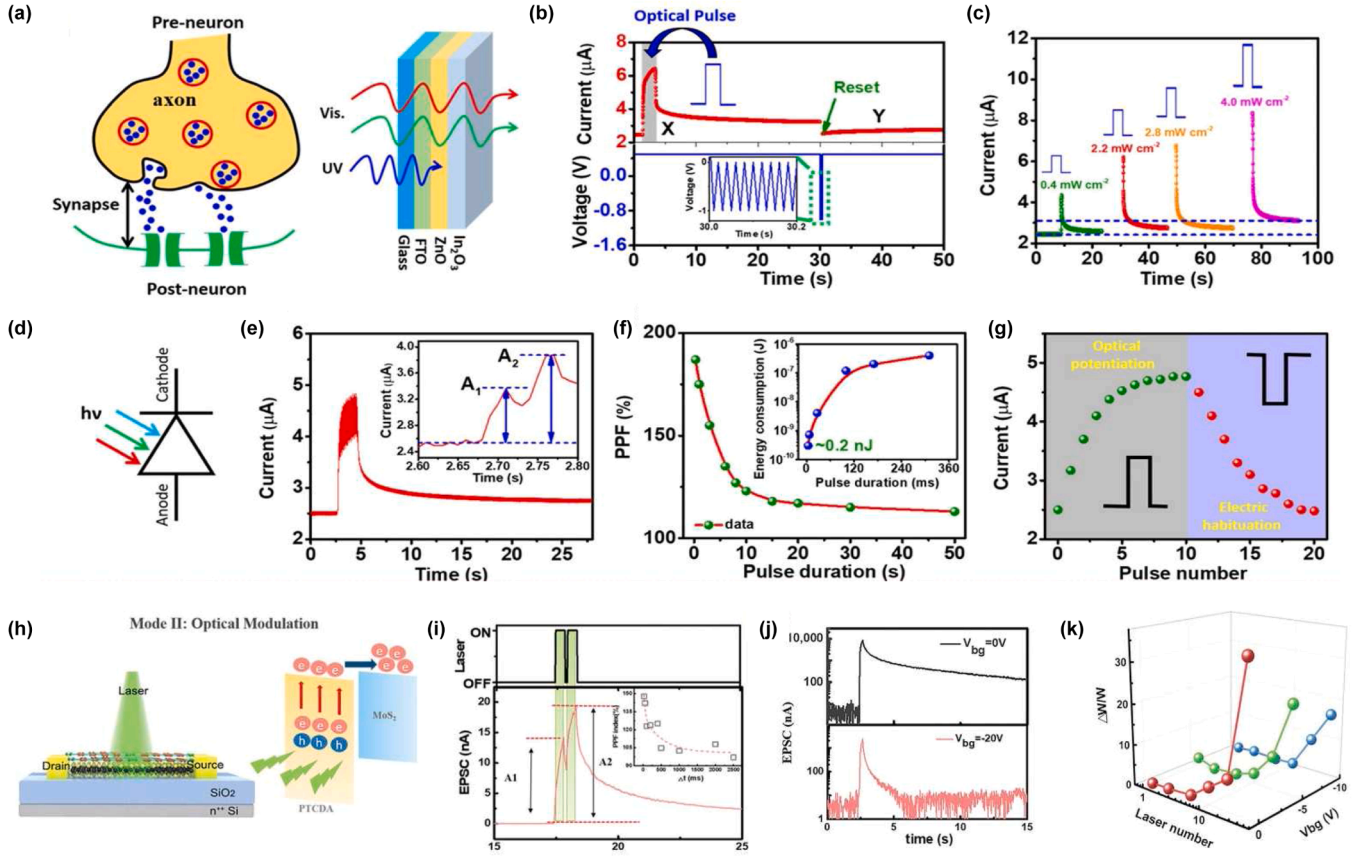

Fig. 10. ZnO based two-terminal and three terminal photonic synapses. (a) Schematics of a synapse structure within the human brain, and ZnO based two-terminal visible light transparent device, respectively. (b) Top panel shows the transient responses of the device after illumination with a single optical pulse (intensity: 0.4 mW cm^{-2}, duration: 2 s, marked by the gray colored area), showing a gradual decay after the UV is switched off (point X). The bottom panel depicts the applied measuring voltage (0.6 V) and pulses of −1 V after 30 s; the inset shows the shape of the applied electric pulses. (c) Transient current–time characteristics for four optical pulses with different intensities from 0.4 to 4 mW cm^{-2}, showing the dynamic behavior of current with the increasing incident light intensity of a single pulse. (d) Sketch of a photodetector, which is very similar to the artificial synapse. (e) Change in the current under the action of applied sequential optical pulses. The inset shows the change in current amplitude for two sequential optical pulses. (f) Change in the PPF index with different optical frequencies. The inset shows the energy consumed per synaptic event as a function of optical pulse duration. (g) Gradual current change across the synaptic devices after applying a train of photonic pulses (intensity: 0.4 mW cm^{-2}, duration and separation: 1 s) and negative electrical pulses (−1 V, duration and separation: 20 ms). Top and bottom insets show the shape of the applied pulses. (a–g) Reproduced with permission [30]. Copyright 2018, American Chemical Society. (h) Optical device architecture schematic and band alignment of heterojunction of the MoS_2 based device. The photogating effect and charge transfer under laser pulse are shown in band structure. (i) EPSC of the MoS_2/PTCDA transistor triggered by a pair of laser pulses. Pulse width 400 ms, interval 100 ms, V_{ds} is 0.1 V, green area represents laser pulses irradiation. The inset is corresponding PPF index A_2/A_1 (black hollow square) as a function of laser pulse interval time (Δt). (j) STP ($V_{bg} = -20$ V) to LTP ($V_{bg} = 0$ V) transition through V_{bg} modulation. (k) The long-term weight change of the synaptic transistor based on MoS_2/PTCDA under different V_{bg} as a function of the laser number, where the laser pulse width, interval, and V_{ds} are kept constant at 100 ms, 25 ms, 1 V, respectively. (a–d) Reproduced with permission [38]. Copyright 2019, John Wiley and Sons. (For interpretation of the references to color in this figure legend, the reader is referred to the web version of this article.)

(HRTEM) image in Fig. 11(b) shows the layered architecture of $CsPbBr_3$ nanoplates. In this particular device structure, conductance modulation is attributed to the interfacial trapping and de-trapping of photo-generated charges. The devices were able to successfully emulate biological synapses, exhibiting enhanced conductance with increasing illumination intensity and duration, as shown in Fig. 11(c) and (d). Three-terminal phototransistors using perovskite have also been utilized as photonic synapses, with one of the pioneering works reported by Pradhan et al. [39]. They successfully fused the optoelectronic properties of perovskite quantum dots with the charge transport properties of graphene to develop an ultra-thin phototransistor comprising HP quantum dots growing from a graphene lattice. The device achieved a responsivity of 1.4×10^8 AW^{-1} and specific detectivity of 4.72×10^{15} Jones at 430 nm illumination. The light/dark current plot and the photocurrent induced LTP retention are represented in Fig. 11(e) and (f). The devices successfully exhibited synaptic traits, including optical potentiation and electrical depression (Fig. 11(g)), along with gate voltage-dependent synaptic strength modulation, as seen in Fig. 11(h).

Image pre-processing and applications in neuromorphic visual systems

In addition to basic STP and LTP emulation, two- and three-terminal photonic synapses have been extensively used to mimic the learning, forgetting, and memorizing tasks performed by the human visual system. Ma et al. demonstrated this concept with an HP photonic synapse-based device that exhibited learning/re-learning and forgetting traits similar to the biological system (Fig. 12(a)–(d)) [31]. The material design and working mechanism of this device are discussed in the previous section (Fig. 11(a)–(d)). Fig. 12(d) shows that the re-learning process was demonstrated such that, under the same illumination intensity and biasing, the learning rate is enhanced due to faster charge trapping at the interfaces. As illustrated in Fig. 12(e)–(g), the originally learned pattern could be retraced after forgetting by using the same illumination intensity, and the retracing became more observable with enhanced external biasing. Photonic synapses are also extensively used to improve the accuracy of computing by performing pre-processing tasks, such as contrast enhancement and noise reduction of perceived

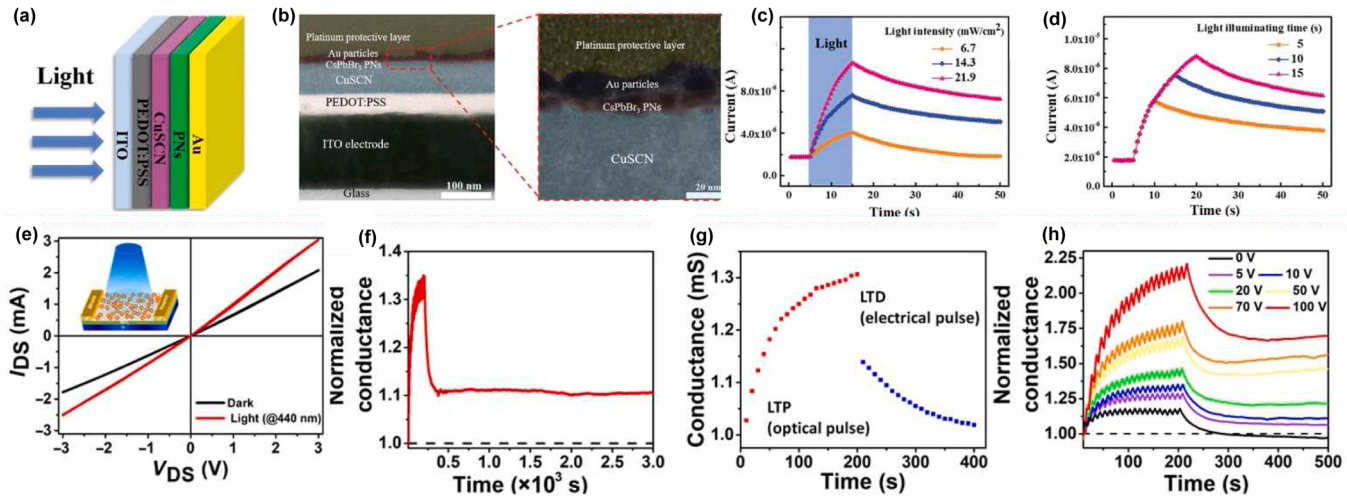

Fig. 11. Perovskite based two-terminal and three terminal photonic synapses. (a) Schematic illustrating the structure of and the test method for the two-terminal perovskite synapse. (b) Cross-sectional TEM image of $CsPbBr_3$ PNs. Cross-sectional TEM image on scales of 100 nm and 20 nm. Photonic PPF index versus time interval between successive pulses. Current–time characteristics for optical pulses with (c) different intensities and (d) different illuminating times. All the read voltages are 0.1 V. (a–d), Reproduced with permission [31]. Copyright 2020, John Wiley and Sons. (e) Perovskite phototransistor drain current (I_{DS}) versus drain voltage (V_{DS}) characteristic of the phototransistor under the dark and illumination intensity of 440 nm monochromatic light with zero gate voltage. Inset: Schematic of G-PQD superstructure phototransistor. (f) Retention of the long-term potentiated device (V_D = 0.5 V and V_G = 10 V) for 3×10^3 s after application of 20 optical pulses (on and off time of 5 and 5 s, respectively). (g) Nonvolatile synaptic plasticity of the device (V_G = = 10 V) showing LTP by train of optical pulses (on and off time of 5 and 5 s, respectively) at V_D = = 0.5 V and LTD by a train of electrical pulses (−0.5 V, on and off time of 1 and 1 s, respectively) at V_D. (h) Gate-dependent transient characteristic of the device (V_D = = 0.5 V) after application of 20 optical pulses (on and off time of 5 and 5 s, respectively). (e–h) Reproduced with permission [39]. Copyright 2020, American Association for the Advancement of Science.

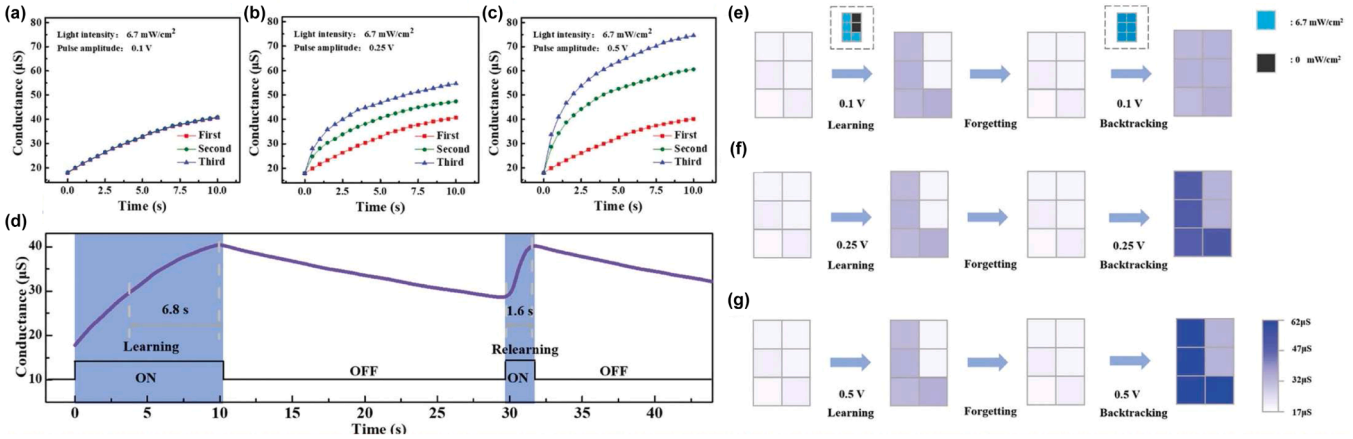

Fig. 12. External-voltage-modulated optical response and learning-experience behavior in perovskite synapses. The conductance evolution of the optoelectronic synapse under three cycles of testing with different amplitudes of (a) 0.1, (b) 0.25, and (c) 0.5 V. (d) The measured learning-experience behavior under a pulsed light stimulus (intensity: 6.7 mW cm^{-2}). Demonstration of memory backtracking function by using a 3 × 2 optoelectronic synapse array. The memory backtracking process can be divided into three stages, namely, learning, forgetting, and backtracking. Voltage pulses with different amplitudes of (e) 0.1, (f) 0.25, and (g) 0.5 V were applied in the learning and the backtracking processes. (a–g) Reproduced with permission [31]. Copyright 2020, John Wiley and Sons.

patterns and images. The specific advantage of using photonic synapses over traditional photodetectors in pre-processing tasks stems from their ability to exhibit simultaneous light sensing, light tunability, and temporal plasticity. Zhou et al. fabricated an 8 by 8 optoelectronic synaptic array based on molybdenum oxide (MoOx) that could demonstrate image memorization, as shown in Fig. 13(a)–(c) [37], and pre-processing functions such as contrast enhancement, as shown in Fig. 13(d) and (e). As shown in Fig. 13(f)–(h), it was further demonstrated that contrast-enhanced letter images led to higher neuromorphic processing accuracy, with an improvement of 41.5 % and a recognition rate of 0.99 when compared to devices without the pre-processing photonic synapse array. It should be noted that recently, flexible synaptic arrays of larger dimensions (32 × 32) and curved synaptic arrays have also been reported, exhibiting neuromorphic pre-processing characteristics [16,32]. These advancements in photonic synapses offer promising prospects for the development of neuromorphic visual systems that can potentially enhance the performance and energy efficiency of image and pattern recognition tasks in various applications, such as robotics, autonomous vehicles, and surveillance systems.

Neuromorphic imaging systems based on curved image sensors

Neuromorphic imaging systems based on curved image sensors offer promising prospects for highly efficient and miniaturized imaging systems inspired by the human visual system. These systems integrate image sensing and neuromorphic pre-processing functions on a single device, simplifying the imaging system and reducing energy consumption. The hemispherical geometry of the sensor can further miniaturize

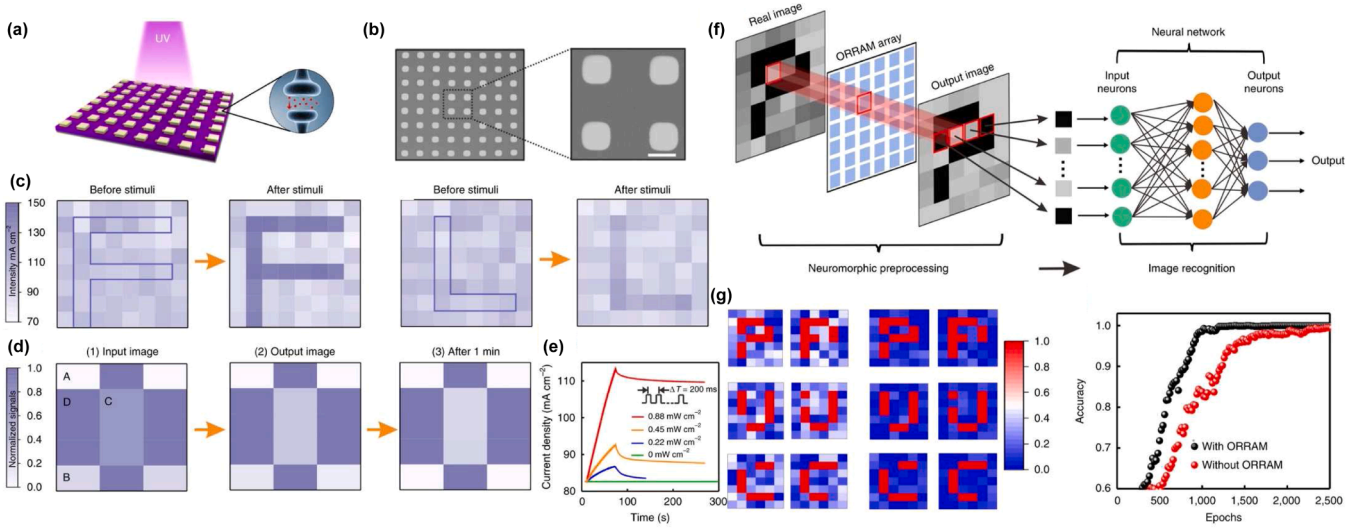

Fig. 13. Photonic synapse enhanced pattern recognition application. (a) Schematic structure of an 8 × 8 ORRAM array. (b) SEM image of an 8 × 8 ORRAM array. Scale bar, 200 μm. (c) Illustrations of the image memory of the letter F and the letter L. The letter F was stimulated with a light intensity of 0.88 mW cm^{-2} and the letter L with a lower light intensity of 0.45 mW cm^{-2} (pulse width, 200 ms; pulse interval, 200 ms). (d) An illustration of the image contrast enhancement after the training processes and the current response e, during and after the training processes. The training process was conducted through an input image repeated 100 times with a frequency of 2.5 Hz (pulse width, 200 ms; pulse interval, 200 ms). The four gray scales in the input image correspond to four light intensities (0 (A), 0.22 (B), 0.45 (C) and 0.88 (D) mW cm^{-2}). The signals in the output image correspond to the current after the training process. The input signals (light intensity) and output signals (current density) were normalized. (f) Illustration of an artificial neuromorphic visual system based on the ORRAM devices for image preprocessing and an artificial neural network for image recognition. (g) Examples of images before (left columns) and after (right columns) ORRAM-based pre-processing. (h) Comparisons of the image recognition rate with and without ORRAM-based image preprocessing. a-h, Reproduced with permission [37]. Copyright 2019, Springer Nature.

the optical sub-system and replicate most functions of the human vision and recognition system in artificial intelligent applications, as shown in Fig. 14(a) [16].

Choi et al. developed a visual system based on a curved neuromorphic image sensor array, inspired by the human eyeball structure and visual recognition system [16]. Fig. 14(b) shows the schematic of such a system. A plano-convex lens serves to focus light onto the curved neuromorphic image sensor. For the curved geometry to fit the curved focal plane, the system can acquire low aberration images. Because of the integration of image sensing and neuromorphic pre-processing functions, the retina can detect objects in a noisy optical environment. The curved image sensor is a mechanically deformable array with a strain-releasing mesh design based on ultrathin and flexible materials. The sensing units are based on a MoS_2-poly(1,3,5-trimethyl-1,3,5-trivinylcyclotrisiloxane) (pV3D3) heterostructure. Fig. 14(c) shows the device structure of one sensing pixel and the energy band diagram of the MoS_2-pV3D3 heterostructure. Because the MoS_2-pV3D3 heterostructure has a type-II band alignment and a large conduction band energy difference, photogenerated electron-hole pairs can be efficiently separated and localized near the respective interface. Hence, the gradual increase of electron and hole density can induce a gradual increase in photocurrent by the photogating effect. Fig. 14(d) shows the shape of the letters C and N detected by the system and related pixel photocurrent curves. With more stimuli, activated pixels can be set to higher photocurrent states. A clearer shape with a higher contrast difference can be acquired by the system. This result shows the successful integration of image sensing and neuromorphic preprocessing functions on the curved retina.

Hu et al. also reported a neuromorphic visual system with a human eyeball inspired structure [21]. Fig. 14(e) shows the schematic of the biomimetic eye system. It also has a fixed lens to focus light and a hemispherical retina to detect the image. The hemispherical neuromorphic image sensor is fabricated by depositing materials on a hemispherical quartz substrate via vapor processes. The sensing units are based on In/MoS_2 heterostructures. Under illumination, photoelectrons generated in the MoS_2 channel are trapped in the multilayer MoS_2 film and slowly released, resulting in a synaptic photo response. As shown in Fig. 14(f), electrons injected from In can significantly increase the conductivity of MoS_2, giving rise to a stronger signal. Fig. 14(g) shows the learning and forgetting process of the system in response to stimuli (the shape of an H).

However, current neuromorphic imaging systems with curved geometry have relatively low resolution and can only recognize simple patterns. Further research is needed to improve the resolution and complexity of these systems to enhance their applicability in various fields, such as robotics, autonomous vehicles, and surveillance systems. Nonetheless, the development of neuromorphic imaging systems based on curved image sensors is a significant step towards achieving highly efficient and miniaturized imaging systems inspired by the human visual system.

Performance parameters for photonic synapses

In previous sections, we delved into the material designs and neuromorphic processing functions of typical photonic synapses. These aspects underscore their efficient in-device computing potential, making them promising for a range of artificial intelligence applications. In this section, we will introduce performance parameters that aid in evaluating various photonic synaptic devices. These parameters will also underline their significance across different application fields.

Synaptic plasticity, the foundational function of both biological and artificial synapses, is viewed as the cornerstone of neuromorphic signal processing. The two principal forms of synaptic plasticity are STP and LTP. STP represents a temporary synaptic connection that stores information briefly, with the connection strength gradually decaying over time. A typical manifestation of STP is PPF, which refers to the enhancement of the postsynaptic response achieved by applying a pair of presynaptic spikes consecutively. Given sufficiently strong or rapid stimulation, STP can transition to LTP, indicating the establishment of a relatively robust connection between the pre synapse and post synapse.

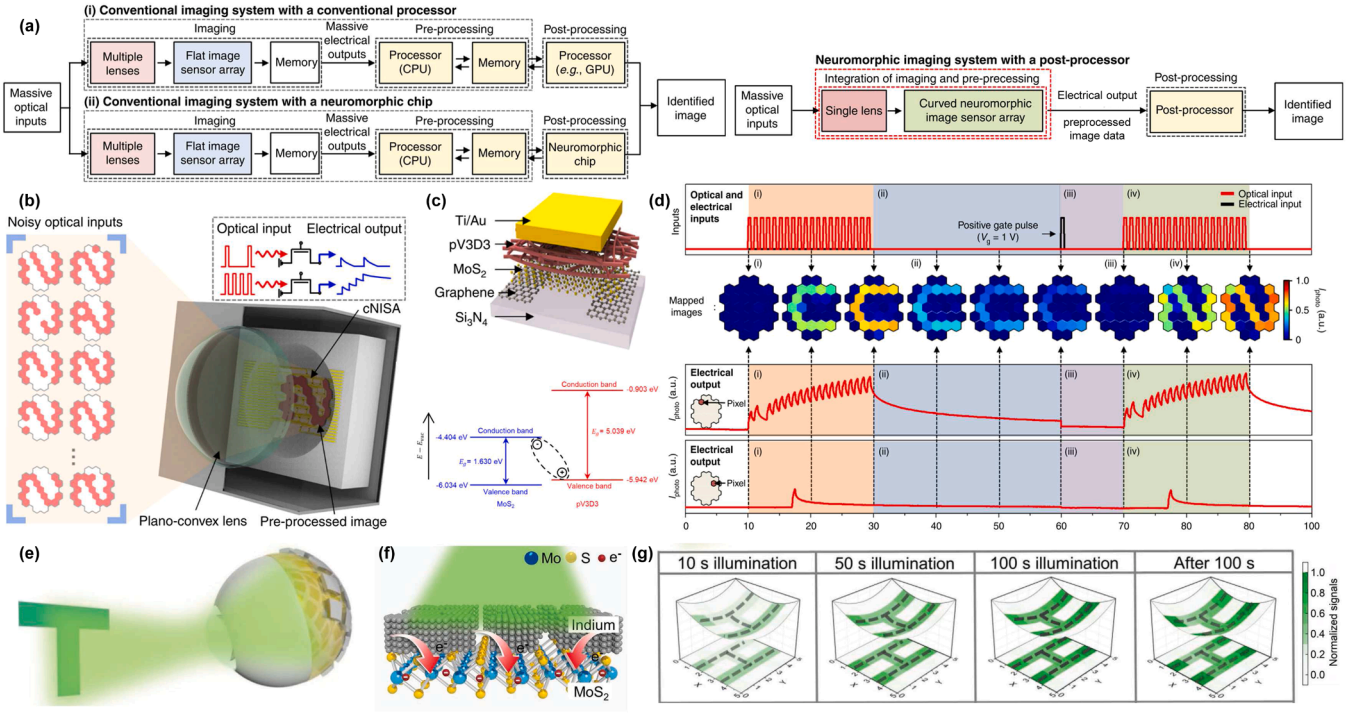

Fig. 14. Neuromorphic imaging systems based on curved image sensors. (a) Block diagrams showing the sequence of the image recognition using the conventional imaging and data processing system (e.g., conventional imaging system with a conventional processor (top) or with a neuromorphic chip (bottom)). And block diagram showing the sequence of the image recognition using cNISA and a post-processor (e.g., GPU or neuromorphic chip). (b) Schematic illustration of the curved neuromorphic imaging device. The inset in the dashed box shows the concept of photon-triggered synaptic plasticity that derives a weighted electrical output from massive optical inputs. (c) Schematic illustration of the device structure and energy band diagram of MoS_2-pV3D3 heterostructure. (d) Demonstrations for deriving a pre-processed image from massive noisy optical inputs (e.g., acquisition of a pre-processed C-shape image (i), decay of the memorized C-shape image (ii), erasure of the afterimage (iii), and acquisition of a pre-processed N-shape image (iv)). (a–d) Reproduced with permission [16]. Copyright 2020, Springer Nature. (e) Schematic structure of hemispherical electronic eye imaging system consisting of a 5 × 5 MoS_2 synaptic devices array. (f) Schematic illustration of the surface charge doping procedure in In/MoS_2 synaptic device. (g) Illustrations of the imaging function of the letter H under 10, 50, and 100 s illumination and for waiting 100 after 100 s illumination with light wavelength of 550 nm and light intensity of 23.6 mW cm^{-2} at a voltage of 0.4 mV, respectively. (e–g) Reproduced with permission [21]. Copyright 2020, John Wiley and Sons.

Both STP and LTP are fundamental to learning and memory functions in neuromorphic computing.

Application scenarios play a crucial role in evaluating photonic synapses. Given the diverse requirements for signal acquisition and processing across various fields, the potential of different devices can vary significantly according to the specific field of application. Currently, the development of most photonic synaptic devices is primarily aimed at enhancing the efficiency of static pattern recognition systems, specifically in fields such as pattern recognition, face recognition, and motion detection.

In Table 2, we showcase a thorough comparison of diverse photonic synapses. This table compiles the key performance parameters for each device, offering a juxtaposed analysis that illuminates their individual strengths and features.

Potential applications of bio-inspired visual systems

In the above sections we reviewed the basic characteristics and advancement of bio-inspired visual systems. The miniaturized, high quality imaging ability based on curved image sensors, and the effective signal processing of neuromorphic hardware are both highly desired for next generation artificial vision related applications. In this section, we will discuss the significances of bio-inspired visual systems through some specific applications. In this section, we will delve deeper into the implications and significance of these bio-inspired visual systems. We aim to highlight their potential through some specific use cases, thereby providing a comprehensive understanding of their transformative capacity in the realm of artificial vision.

Visual systems occupy a critical role in the operation of autonomous platforms, such as drones and autonomous vehicles, serving as an indispensable element that enables various functions such as navigation [85], obstacle avoidance [86], and imaging [87]. Curved image sensors based imaging systems, which are lightweight and miniaturized, offer wide Field of View (FoV) imaging capabilities making them highly suitable for these applications [87]. A wide FoV system can capture an expansive view of the surroundings, providing these autonomous platforms with a wealth of information that aids in navigation through complex environments [88]. Furthermore, such platforms can better anticipate and react to environmental factors that may impact their stability during operation. Simultaneously, the reduction in weight and energy consumption inherent in these miniaturized systems presents the potential to enhance endurance, a particularly significant benefit for drones [89].

Extended Reality (XR), encompassing the fusion of digital and physical realities, holds the potential to transform how individuals interact with their surroundings [90]. Imaging technologies are regarded as one of the cornerstones of XR technologies, given the paramount role of visual information in recognizing and interacting with objects [91]. Bio-inspired visual systems, which capture images in a manner akin to the human eye, can provide a more natural visual experience and foster more compatible interfaces. The advanced attributes of these bio-inspired visual systems, such as human eye-like imaging, precise object recognition, and energy efficiency, can substantially contribute to the advancement of related technologies.

Pattern recognition is a powerful function of a visual system that can be used in diversified applications including image analysis [92–94],

Table 2
Summary of typical photonic synapses.

Device structure	Active layer	STP	LTP	Application demonstration	Ref.
Two terminals	ZnO	√	√	–	[41]
Two terminals	ZnO	√		–	[40]
Two terminals	ZnO	√	√	–	[30]
Three terminals	ZnO	√	√	–	[42]
Three terminals	ZnO	√	√	Pattern recognition	[33]
Three terminals	IGZO	√	√	–	[27]
Two terminals	MoO_x	√	√	Pattern recognition	[37]
Two terminals	MoS_2	√	√	Curved image sensor / Pattern recognition	[16]
Three terminals	MoS_2/PTCDA	√	√	–	[38]
Two terminals	$CsPbBr_3$	√	√	Pattern recognition	[31]
Three terminals	$CsPbBr_3$/CNT	√	√	Pattern recognition	[32]
Two terminals	$MAPbBr_3$/ MWCNT	√	√	Pattern recognition	[43]
Three terminals	$MAPbBr_3$	√	√	Face recognition	[39]
Three terminals	BA_2PbBr_4	√	√	Pattern recognition	[29]

security [95–97], and healthcare [98–100]. A conventional pattern recognition system comprises image sensors, preprocessors, and processors based on artificial neural networks (ANN) [16]. The enhancement of pattern recognition capabilities through the integration of neuromorphic hardware has been extensively documented [101–104]. By utilizing bio-inspired systems, which are proficient at acquiring extensive information from a scene and processing signals with high efficiency, the performance of pattern recognition systems can be substantially enhanced to support the rapid development of artificial intelligence.

Generally, bio-inspired visual systems demonstrate robust proficiency in capturing and processing visual information, thereby unlocking vast potential across a broad spectrum of applications. These systems draw inspiration from biological entities, leveraging the strengths of natural vision systems to enhance perceptual and interpretative capacities in artificial systems. However, the path towards fully realizing the potential of bio-inspired visual systems is not without challenges. In the following section, we will delve into these hurdles while also exploring future prospects.

Challenges and future prospect of bio-inspired visual systems

While bio-inspired visual systems exhibit remarkable capabilities, they are not exempt from challenges. In this section, we will explore the current limitations within this field, as well as consider future directions and potential advancements.

Achieving high resolution remains a significant challenge for curved image sensors, especially those with a high degree of curvature. The rigidity of silicon material makes it difficult to deform curved CMOS devices into a geometry with a curvature degree exceeding 30°. Designs that are stretchable and foldable can potentially address stress-related issues, but the components involved in bending aren't light-sensitive, which restricts the increase in pixel density. Hemispherical nanowire array devices can achieve a diffraction-limited integration of photo sensing units. At present, a hemispherical device can barely achieve a pixel density higher than 200 pixels per inch or a resolution exceeding 2000 pixels. Obtaining sufficient detail in the scene is crucial for curved image sensors in practical applications, making high resolution a key performance metric. Therefore, addressing these resolution constraints represents a priority in the ongoing development and optimization of curved image sensors.

The current cutting-edge curved image sensors primarily rely on broadband image sensors. However, our world is abundant with color, bathed in illumination of varying wavelengths. A bio-inspired visual system with color imaging capability could detect objects in a manner more similar to the human eye. At present, fabricating a color filter array on a curved substrate poses considerable challenges. The development of color-sensitive photo sensing devices may be a viable solution to this challenge [23]. By integrating these color-sensitive sensors on the curved geometry, we could potentially enhance the system's ability to accurately and vividly capture the colorful world around us. This advancement would not only enrich the visual data obtained but also bring us a step closer to creating artificial visual systems that truly mimic human vision.

Photonic synapses excel in processing static visual information, including patterns, shapes, and objects. Yet, the challenge remains in effectively detecting and processing motion information [45,105]. Drawing inspiration from human vision, event-based neuromorphic image sensors have been developed using complex structures found in conventional electronics [106,107]. By emulating the efficient detection and processing of motion information characteristic of animal vision, we may potentially develop a bio-inspired visual system in the future. This system, with a simplified structure and efficient motion sensing, could significantly advance our capabilities in dynamic visual data processing.

Moreover, the development of neuromorphic hardware with curved geometries is not commonly reported. The fabrication of materials and circuits on curved substrates presents significant challenges, largely due to current manufacturing limitations. The integration of potent imaging capabilities with efficient signal processing could yield significantly enhanced features. Therefore, the invention of new designs and fabrication methods is highly desirable.

While bio-inspired visual systems hold immense potential, significant challenges still persist. It is our hope that this review will inspire talented researchers to join the collective effort in resolving these challenges and advancing the development of even more powerful bio-inspired visual systems.

Summary

Future applications of machine vision demand imaging systems with low aberration, wide FoV, miniaturization, and energy efficiency. However, conventional visual systems are limited by their planar detectors and separated functional modules. In contrast, biological visual systems with curved retinas and neuromorphic computing abilities provide inspiration for developing novel artificial visual systems. In this paper, we review state-of-the-art bio-inspired visual systems based on curved image sensors and photonic synapses.

Curved image sensors can correct the mismatch between planar detector geometry and Petzval field curvature, allowing for high-quality imaging with simplified lenses. Promising methods such as mechanical deformation, compressible and stretchable island-bridge structures, origami and kirigami designs, buckling-guided assembly, template-assisted growth, and 3D-surface printing have been developed to fabricate curved image sensors. Low-aberration imaging systems inspired by human, aquatic, and arthropod eyes have been reported based on concave and convex image sensors. By mimicking biological eye structures, bio-inspired eyes can have attractive features such as a wide FoV, expanded depth of field, and a large dynamic range. However, state-of-the-art curved image sensors are limited by low resolution and poor color selectivity.

Biological visual systems have synapses for neuromorphic signal preprocessing, storage, retrieval, and processing. Artificial photonic synapses with both light-sensing and neuromorphic pre-processing

abilities can simplify conventional visual systems. By integrating the functions of image sensing, storage, and pre-processing into a single chip, these systems can reduce energy consumption by removing redundant modules and signal communications. We reviewed state-of-the-art photonic synapses with two-terminal and three-terminal device structures, and traditional oxides, sulfides, and perovskites are promising candidates for photonic synapses. Photonic synapse-based visual systems can learn/re-learn, memorize, and forget external visual information, enabling them to detect and process visual information with faster speed, higher accuracy, and less energy consumption. Commercial applications require photonic synapses with higher light sensitivity and stability, lower energy consumption, and high-resolution photonic synapse arrays.

The combination of curved sensor geometry and photonic synaptic ability is ideal for bio-inspired visual systems. We reviewed typical curved neuromorphic image sensor-based visual systems, which can acquire low aberration, wide FoV images with a single lens and pre-process visual information simultaneously. However, state-of-the-art curved neuromorphic image sensors are also limited by low resolution.

Overall, curved image sensors can overcome the aberration in conventional cameras and simplify optical elements, while photonic synapses can remove redundant modules and reduce energy consumption. Inspired by distinctive biological visions, promising visual systems based on curved sensor geometry and/or photonic synapses have been demonstrated. However, low resolution and poor color selectivity have limited the commercialization of biomimetic optoelectronic devices. Additionally, achieving effective motion detection capability remains a considerable challenge in the development of bio-inspired visual systems. We hope that this review will inspire and motivate more researchers to develop the next generation of manufacturable visual systems based on biomimetic designs.

Declaration of Competing Interest

The authors declare that they have no known competing financial interests or personal relationship appeared to influence the work reported in this paper.

Data availability

No data was used for the research described in the article.

Acknowledgments

This work was supported by the Science and Technology Plan of Shen Zhen (JCYJ20170818114107730, JCYJ20180306174923335), The General Research Fund (projects 16205321, 16214619) from the Hong Kong Research Grant Council, Innovation Technology Fund (GHP/014/19SZ), Guangdong-Hong Kong-Macao Intelligent Micro-Nano Optoelectronic Technology Joint Laboratory (project 2020B1212030010), and Foshan Innovative and Entrepreneurial Research Team Program (2018IT100031). We also acknowledge the support from the Center for 1D/2D Quantum Materials and the State Key Laboratory of Advanced Displays and Optoelectronics Technologies at HKUST. Z. F. acknowledges the support from the New Cornerstone Science Foundation through the XPLORER PRIZE and Hong Kong Alliance of Technology and Innovation through BOCHK Science and Technology Innovation Prize.

References

[1] W.-L. Liang, J.-G. Pan, G.-D.J. Su, Optica 6 (2019) 326.
[2] A. Arbabi, E. Arbabi, S.M. Kamali, Y. Horie, S. Han, A. Faraon, Nat. Commun. 7 (2016) 13682.
[3] B. Ma, K. Sharma, K.P. Thompson, J.P. Rolland, Opt. Express 21 (2013) 17454.
[4] X. Li, J. Suo, W. Zhang, X. Yuan, Q. Dai, in: 2021 IEEE/CVF Int. Conf. Comput. Vis., IEEE, 2021, pp. 2593–2601.
[5] S. Chen, H. Feng, D. Pan, Z. Xu, Q. Li, Y. Chen, ACM Trans. Graph. 40 (2021) 1–15.
[6] Y. Chai, Nature 579 (2020) 32–33.
[7] F. Ankel-Simons, D.T. Rasmussen, Am. J. Phys. Anthropol. 137 (2008) 100–117.
[8] M.S. Kim, M.S. Kim, G.J. Lee, S. Sunwoo, S. Chang, Y.M. Song, D. Kim, Adv. Mater. Technol. 7 (2022), 2100144.
[9] I. Jung, J. Xiao, V. Malyarchuk, C. Lu, M. Li, Z. Liu, J. Yoon, Y. Huang, J. A. Rogers, Proc. Natl. Acad. Sci. USA 108 (2011) 1788–1793.
[10] H.C. Ko, M.P. Stoykovich, J. Song, V. Malyarchuk, W.M. Choi, C.-J. Yu, J. B. Geddes III, J. Xiao, S. Wang, Y. Huang, J.A. Rogers, Nature 454 (2008) 748–753.
[11] K. Itonaga, T. Arimura, K. Matsumoto, G. Kondo, K. Terahata, S. Makimoto, M. Baba, Y. Honda, S. Bori, T. Kai, K. Kasahara, M. Nagano, M. Kimura, Y. Kinoshita, E. Kishida, T. Baba, S. Baba, Y. Nomura, N. Tanabe, N. Kimizuka, Y. Matoba, T. Takachi, E. Takagi, T. Haruta, N. Ikebe, K. Matsuda, T. Niimi, T. Ezaki, T. Hirayama, in: 2014 Symp. VLSI Technol. Dig. Tech. Pap., IEEE, 2014, pp. 1–2.
[12] B. Guenter, N. Joshi, R. Stoakley, A. Keefe, K. Geary, R. Freeman, J. Hundley, P. Patterson, D. Hammon, G. Herrera, E. Sherman, A. Nowak, R. Schubert, P. Brewer, L. Yang, R. Mott, G. McKnight, Opt. Express 25 (2017) 13010.
[13] Y.M. Song, Y. Xie, V. Malyarchuk, J. Xiao, I. Jung, K.-J. Choi, Z. Liu, H. Park, C. Lu, R.-H. Kim, R. Li, K.B. Crozier, Y. Huang, J.A. Rogers, Nature 497 (2013) 95–99.
[14] C. Choi, M.K. Choi, S. Liu, M.S. Kim, O.K. Park, C. Im, J. Kim, X. Qin, G.J. Lee, K. W. Cho, M. Kim, E. Joh, J. Lee, D. Son, S.-H. Kwon, N.L. Jeon, Y.M. Song, N. Lu, D.-H. Kim, Nat. Commun. 8 (2017) 1664.
[15] K. Zhang, Y.H. Jung, S. Mikael, J.-H. Seo, M. Kim, H. Mi, H. Zhou, Z. Xia, W. Zhou, S. Gong, Z. Ma, Nat. Commun. 8 (2017) 1782.
[16] C. Choi, J. Leem, M. Kim, A. Taqieddin, C. Cho, K.W. Cho, G.J. Lee, H. Seung, H. J. Bae, Y.M. Song, T. Hyeon, N.R. Aluru, S. Nam, D.-H. Kim, Nat. Commun. 11 (2020) 5934.
[17] M.S. Kim, G.J. Lee, C. Choi, M.S. Kim, M. Lee, S. Liu, K.W. Cho, H.M. Kim, H. Cho, M.K. Choi, N. Lu, Y.M. Song, D.-H. Kim, Nat. Electron. 3 (2020) 546–553.
[18] M. Lee, G.J. Lee, H.J. Jang, E. Joh, H. Cho, M.S. Kim, H.M. Kim, K.M. Kang, J. H. Lee, M. Kim, H. Jang, J.-E. Yeo, F. Durand, N. Lu, D.-H. Kim, Y.M. Song, Nat. Electron. 5 (2022) 452–459.
[19] Z. Rao, Y. Lu, Z. Li, K. Sim, Z. Ma, J. Xiao, C. Yu, Nat. Electron. 4 (2021) 513–521.
[20] C. Choi, M.K. Choi, S. Liu, M. Kim, O.K. Park, C. Im, J. Kim, X. Qin, G.J. Lee, K. W. Cho, M. Kim, E. Joh, J. Lee, D. Son, S.-H. Kwon, N.L. Jeon, Y.M. Song, N. Lu, D.-H. Kim, Nat. Commun. 8 (2017) 1664.
[21] Y. Hu, M. Dai, W. Feng, X. Zhang, F. Gao, S. Zhang, B. Tan, J. Zhang, Y. Shuai, Y. Fu, P. Hu, Adv. Mater. 33 (2021), 2104960.
[22] L. Gu, S. Poddar, Y. Lin, Z. Long, D. Zhang, Q. Zhang, L. Shu, X. Qiu, M. Kam, A. Javey, Z. Fan, Nature 581 (2020) 278–282.
[23] Z. Long, X. Qiu, C.L.J. Chan, Z. Sun, Z. Yuan, S. Poddar, Y. Zhang, Y. Ding, L. Gu, Y. Zhou, W. Tang, A.K. Srivastava, C. Yu, X. Zou, G. Shen, Z. Fan, Nat. Commun. 14 (2023) 1972.
[24] Y. Ding, G. Liu, Z. Long, Y. Zhou, X. Qiu, B. Ren, Q. Zhang, C. Chi, Z. Wan, B. Huang, Z. Fan, Sci. Adv. 8 (2022) 31.
[25] S. Cohen-Cory, Science 298 (2002) 770–776 (80-.).
[26] J. Zhang, S. Dai, Y. Zhao, J. Zhang, J. Huang, Adv. Intell. Syst. 2 (2020), 1900136.
[27] Y. He, S. Nie, R. Liu, S. Jiang, Y. Shi, Q. Wan, IEEE Electron Device Lett. 40 (2019) 818–821.
[28] Y. Wang, L. Yin, W. Huang, Y. Li, S. Huang, Y. Zhu, D. Yang, X. Pi, Adv. Intell. Syst. 3 (2021), 2000099.
[29] Y. Park, M.-K. Kim, J.-S. Lee, J. Mater. Chem. C 9 (2021) 1429–1436.
[30] M. Kumar, S. Abbas, J. Kim, ACS Appl. Mater. Interfaces 10 (2018) 34370–34376.
[31] F. Ma, Y. Zhu, Z. Xu, Y. Liu, X. Zheng, S. Ju, Q. Li, Z. Ni, H. Hu, Y. Chai, C. Wu, T. W. Kim, F. Li, Adv. Funct. Mater. 30 (2020), 1908901.
[32] Q.-B. Zhu, B. Li, D.-D. Yang, C. Liu, S. Feng, M.-L. Chen, Y. Sun, Y.-N. Tian, X. Su, X.-M. Wang, S. Qiu, Q.-W. Li, X.-M. Li, H.-B. Zeng, H.-M. Cheng, D.-M. Sun, Nat. Commun. 12 (2021) 1798.
[33] C. Shen, X. Gao, C. Chen, S. Ren, J.-L. Xu, Y.-D. Xia, S.-D. Wang, Nanotechnology 33 (2022), 065205.
[34] N.-G. Park, Mater. Today 18 (2015) 65–72.
[35] H. Han, H. Yu, H. Wei, J. Gong, W. Xu, Small 15 (2019), 1900695.
[36] S.-F. Leung, K.-T. Ho, P.-K. Kung, V.K.S. Hsiao, H.N. Alshareef, Z.L. Wang, J.-H. He, Adv. Mater. 30 (2018), 1704611.
[37] F. Zhou, Z. Zhou, J. Chen, T.H. Choy, J. Wang, N. Zhang, Z. Lin, S. Yu, J. Kang, H.-S.P. Wong, Y. Chai, Nat. Nanotechnol. 14 (2019) 776–782.
[38] S. Wang, C. Chen, Z. Yu, Y. He, X. Chen, Q. Wan, Y. Shi, D.W. Zhang, H. Zhou, X. Wang, P. Zhou, Adv. Mater. 31 (2019), 1806227.
[39] B. Pradhan, S. Das, J. Li, F. Chowdhury, J. Cherusseri, D. Pandey, D. Dev, A. Krishnaprasad, E. Barrios, A. Towers, A. Gesquiere, L. Tetard, T. Roy, J. Thomas, Sci. Adv. 6 (2020) eaay5225.
[40] W. Zhou, R. Yang, H.-K. He, H.-M. Huang, J. Xiong, X. Guo, Appl. Phys. Lett. 113 (2018), 061107.
[41] Y. Zhu, C. Wu, Z. Xu, Y. Liu, H. Hu, T. Guo, T.W. Kim, Y. Chai, F. Li, Nano Lett. 21 (2021) 6087–6094.
[42] J.-Y. Mao, L. Hu, S.-R. Zhang, Y. Ren, J.-Q. Yang, L. Zhou, Y.-J. Zeng, Y. Zhou, S.-T. Han, J. Mater. Chem. C 7 (2019) 48–59.
[43] J. Li, P. Dwivedi, K.S. Kumar, T. Roy, K.E. Crawford, J. Thomas, Adv. Electron. Mater. 7 (2021), 2000535.

[44] S. Seo, S.-H. Jo, S. Kim, J. Shim, S. Oh, J.-H. Kim, K. Heo, J.-W. Choi, C. Choi, S. Oh, D. Kuzum, H.-S.P. Wong, J.-H. Park, Nat. Commun. 9 (2018) 5106.
[45] J. Chen, Z. Zhou, B.J. Kim, Y. Zhou, Z. Wang, T. Wan, J. Yan, J. Kang, J.-H. Ahn, Y. Chai, Nat. Nanotechnol. 18 (2023) 882–888.
[46] Z. Zhang, S. Wang, C. Liu, R. Xie, W. Hu, P. Zhou, Nat. Nanotechnol. 17 (2022) 27–32.
[47] R. Völkel, M. Eisner, K.J. Weible, Microelectron. Eng. 67–68 (2003) 461–472.
[48] M. Ahmad, I. Ahmed, K. Ullah, I. Khan, A. Khattak, A. Adnan, Int. J. Adv. Comput. Sci. Appl. 10 (2019) 522–529.
[49] D. Dumas, M. Fendler, N. Baier, J. Primot, E. Le Coarer, Appl. Opt. 51 (2012) 5419–5424.
[50] J.A. Gregory, A.M. Smith, E.C. Pearce, R.L. Lambour, R.Y. Shah, H.R. Clark, K. Warner, R.M. Osgood, D.F. Woods, A.E. DeCew, S.E. Forman, L. Mendenhall, C. M. DeFranzo, V.S. Dolat, A.H. Loomis, Appl. Opt. 54 (2015) 3072.
[51] S. Shi, L. Yao, P. Ma, Y. Jiao, X. Zheng, D. Ning, M. Chen, F. Sui, H. Liu, C. Yang, W. Li, Mater. Today Energy 20 (2021), 100640.
[52] S. Han, H. Peng, Q. Sun, S. Venkatesh, K. Chung, S.C. Lau, Y. Zhou, V.A.L. Roy, Adv. Mater. 29 (2017), 1700375.
[53] Y. Ji, B. Cho, S. Song, T.-W. Kim, M. Choe, Y.H. Kahng, T. Lee, Adv. Mater. 22 (2010) 3071–3075.
[54] Z. Xue, H. Song, J.A. Rogers, Y. Zhang, Y. Huang, Adv. Mater. 32 (2020) 1–32.
[55] D.H. Kim, J. Song, M.C. Won, H.S. Kim, R.H. Kim, Z. Liu, Y.Y. Huang, K. C. Hwang, Y.W. Zhang, J.A. Rogers, Proc. Natl. Acad. Sci. USA 105 (2008) 18675–18680.
[56] J. Song, Y. Huang, J. Xiao, S. Wang, K.C. Hwang, H.C. Ko, D.H. Kim, M. P. Stoykovich, J.A. Rogers, J. Appl. Phys. (2009), 123516.
[57] J.A. Fan, W.-H. Yeo, Y. Su, Y. Hattori, W. Lee, S.-Y. Jung, Y. Zhang, Z. Liu, H. Cheng, L. Falgout, M. Bajema, T. Coleman, D. Gregoire, R.J. Larsen, Y. Huang, J.A. Rogers, Nat. Commun. 5 (2014) 3266.
[58] W. Lee, Y. Liu, Y. Lee, B.K. Sharma, S.M. Shinde, S.D. Kim, K. Nan, Z. Yan, M. Han, Y. Huang, Y. Zhang, J.-H. Ahn, J.A. Rogers, Nat. Commun. 9 (2018) 1417.
[59] Z. Xu, Z. Fan, W. Pang, Y. Zi, Y. Zhang, Extrem. Mech. Lett. 51 (2022), 101582.
[60] W. Lee, S.J. Park, Chem. Rev. 114 (2014) 7487–7556.
[61] S.-F. Leung, L. Gu, Q. Zhang, K.-H. Tsui, J.-M. Shieh, C.-H. Shen, T.-H. Hsiao, C.-H. Hsu, L. Lu, D. Li, Q. Lin, Z. Fan, Sci. Rep. 4 (2014) 4243.
[62] R. Yu, K.-L. Ching, Q. Lin, S.-F. Leung, D. Arcrossito, Z. Fan, ACS Nano 5 (2011) 9291–9298.
[63] M.M. Tavakoli, L. Gu, Y. Gao, C. Reckmeier, J. He, A.L. Rogach, Y. Yao, Z. Fan, Sci. Rep. 5 (2015) 14083.
[64] A. Waleed, Z. Fan, Sci. Bull. 62 (2017) 645–647.
[65] A. Waleed, M.M. Tavakoli, L. Gu, Z. Wang, D. Zhang, A. Manikandan, Q. Zhang, R. Zhang, Y.L. Chueh, Z. Fan, Nano Lett. 17 (2017) 523–530.
[66] M.M. Tavakoli, A. Waleed, L. Gu, D. Zhang, R. Tavakoli, B. Lei, W. Su, F. Fang, Z. Fan, Nanoscale 9 (2017) 5828–5834.
[67] A. Waleed, M.M. Tavakoli, L. Gu, S. Hussain, D. Zhang, S. Poddar, Z. Wang, R. Zhang, Z. Fan, Nano Lett. 17 (2017) 4951–4957.
[68] L. Gu, D. Zhang, M. Kam, Q. Zhang, S. Poddar, Y. Fu, X. Mo, Z. Fan, Nanoscale 10 (2018) 15164–15172.
[69] Y. Zhou, X. Qiu, Z. Wan, Z. Long, S. Poddar, Q. Zhang, Y. Ding, C.L.J. Chan, D. Zhang, K. Zhou, Y. Lin, Z. Fan, Nano Energy 100 (2022), 107516.
[70] Q. Zhang, D. Zhang, L. Gu, K.H. Tsui, S. Poddar, Y. Fu, L. Shu, Z. Fan, ACS Nano 14 (2020) 1577–1585.
[71] D. Zhang, L. Gu, Q. Zhang, Y. Lin, D.H. Lien, M. Kam, S. Poddar, E.C. Garnett, A. Javey, Z. Fan, Nano Lett. 19 (2019) 2850–2857.
[72] Q. Zhang, M.M. Tavakoli, L. Gu, D. Zhang, L. Tang, Y. Gao, J. Guo, Y. Lin, S.-F. Leung, S. Poddar, Y. Fu, Z. Fan, Nat. Commun. 10 (2019) 727.
[73] L. Gu, M.M. Tavakoli, D. Zhang, Q. Zhang, A. Waleed, Y. Xiao, K.H. Tsui, Y. Lin, L. Liao, J. Wang, Z. Fan, Adv. Mater. 28 (2016) 9713–9721.
[74] B. Seong, H. Yoo, V.D. Nguyen, Y. Jang, C. Ryu, D. Byun, J. Micromech. Microeng. 24 (2014), 097002.
[75] J. Mei, M.R. Lovell, M.H. Mickle, IEEE Trans. Electron. Packag. Manuf. 28 (2005) 265–273.
[76] J.J. Adams, E.B. Duoss, T.F. Malkowski, M.J. Motala, B.Y. Ahn, R.G. Nuzzo, J. T. Bernhard, J.A. Lewis, Adv. Mater. 23 (2011) 1335–1340.
[77] B.W. An, K. Kim, M. Kim, S.Y. Kim, S.H. Hur, J.U. Park, Small 11 (2015) 2263–2268.
[78] D.A. Atchison, G. Smith. Optics of the Human Eye, Butterworth-Heinemann, 2000. https://doi.org/10.1016/B978-0-7506-3775-6.X5001-9.
[79] X. Zhuge, J. Wang, F. Zhuge, Phys. Status Solidi—Rapid Res. Lett. 13 (2019), 1900082.
[80] K. Lin, J. Xing, L.N. Quan, F.P.G. de Arquer, X. Gong, J. Lu, L. Xie, W. Zhao, D. Zhang, C. Yan, W. Li, X. Liu, Y. Lu, J. Kirman, E.H. Sargent, Q. Xiong, Z. Wei, Nature 562 (2018) 245–248.
[81] Y. Zhang, J. Yao, Y. Teng, Z. Zhang, L. Wang, X. Wang, Y. Li, L. Kang, J.-H. He, X. Fang, Nano Energy 117 (2023), 108915.
[82] Y. Zhang, F. Cao, S. Li, X. Liu, L. Kang, L. Wu, X. Fang, J. Mater. Sci. Technol. 129 (2022) 108–114.
[83] Y. Zhang, J. Yao, Z. Zhang, R. Zhang, L. Li, Y. Teng, Z. Shen, L. Kang, L. Wu, X. Fang, J. Mater. Sci. Technol. 164 (2023) 95–101.
[84] Y. Zhu, L. Shu, S. Poddar, Q. Zhang, Z. Chen, Y. Ding, Z. Long, S. Ma, B. Ren, X. Qiu, Z. Fan, Nano Lett. 22 (2022) 9586–9595.
[85] V.J. Hodge, R. Hawkins, R. Alexander, Neural Comput. Appl. 33 (2021) 2015–2033.
[86] K. McGuire, G. de Croon, C. De Wagter, K. Tuyls, H. Kappen, IEEE Robot. Autom. Lett. 2 (2017) 1070–1076.
[87] H. Gupta, O.P. Verma, Multimed. Tools Appl. 81 (2022) 19683–19703.
[88] G.C.H.E. de Croon, J.J.G. Dupeyroux, S.B. Fuller, J.A.R. Marshall, Sci. Robot. 7 (2022) 1–12.
[89] M. Hassanalian, A. Abdelkefi, Prog. Aerosp. Sci. 91 (2017) 99–131.
[90] C. Andrews, M.K. Southworth, J.N.A. Silva, J.R. Silva, Curr. Treat. Options Cardiovasc. Med. 21 (2019) 18.
[91] J. Park, H. Seung, D.C. Kim, M.S. Kim, D. Kim, Adv. Funct. Mater. 31 (2021), 2009281.
[92] S. Nowozin, K. Tsuda, T. Uno, T. Kudo, G. Bakir, in: 2007 IEEE Conf. Comput. Vis. Pattern Recognit, IEEE, 2007, pp. 1–8.
[93] D. Komura, S. Ishikawa, Comput. Struct. Biotechnol. J. 16 (2018) 34–42.
[94] J. Mairal, F. Bach, J. Ponce, G. Sapiro, A. Zisserman, in: 2008 IEEE Conf. Comput. Vis. Pattern Recognit, IEEE, 2008, pp. 1–8.
[95] T. Russ, C. Boehnen, T. Peters, in: 2006 IEEE Comput. Soc. Conf. Comput. Vis. Pattern Recognit 2, IEEE, 2006, pp. 1391–1398.
[96] T.D. Russ, M.W. Koch, C.Q. Little, in: 2005 IEEE Comput. Soc. Conf. Comput. Vis. Pattern Recognit. - Work., IEEE, 2005, p. 169.
[97] P.J. Phillips, P.J. Flynn, T. Scruggs, K.W. Bowyer, J. Chang, K. Hoffman, J. Marques, J. Min, W. Worek, in: 2005 IEEE Comput. Soc. Conf. Comput. Vis. Pattern Recognit., IEEE, 2005, pp. 947–954.
[98] L.D. Cohen, I. Cohen, in: Proc. 1992 IEEE Comput. Soc. Conf. Comput. Vis. Pattern Recognit, IEEE Comput. Soc. Press, 1992, pp. 592–598.
[99] Y. Zheng, B. Georgescu, H. Ling, S.K. Zhou, M. Scheuering, D. Comaniciu, in: 2009 IEEE Conf. Comput. Vis. Pattern Recognit, IEEE, 2009, pp. 194–201.
[100] W. Ma, J.-M. Morel, S. Osher, A. Chien, in: CVPR 2011, IEEE, 2011, pp. 153–160.
[101] S. Oh, J.-J. Lee, S. Seo, G. Yoo, J.-H. Park, Npj 2D Mater. Appl. 5 (2021) 95.
[102] S. Seo, B.-S. Kang, J.-J. Lee, H.-J. Ryu, S. Kim, H. Kim, S. Oh, J. Shim, K. Heo, S. Oh, J.-H. Park, Nat. Commun. 11 (2020) 3936.
[103] S. Park, M. Chu, J. Kim, J. Noh, M. Jeon, B. Hun Lee, H. Hwang, B. Lee, B. Lee, Sci. Rep. 5 (2015) 10123.
[104] K.M. Song, J.-S. Jeong, B. Pan, X. Zhang, J. Xia, S. Cha, T.-E. Park, K. Kim, S. Finizio, J. Raabe, J. Chang, Y. Zhou, W. Zhao, W. Kang, H. Ju, S. Woo, Nat. Electron. 3 (2020) 148–155.
[105] T. Sarkar, K. Lieberth, A. Pavlou, T. Frank, V. Mailaender, I. McCulloch, P.W. M. Blom, F. Torricelli, P. Gkoupidenis, Nat. Electron. 5 (2022) 774–783.
[106] G. Gallego, T. Delbruck, G. Orchard, C. Bartolozzi, B. Taba, A. Censi, S. Leutenegger, A.J. Davison, J. Conradt, K. Daniilidis, D. Scaramuzza, IEEE Trans. Pattern Anal. Mach. Intell. 44 (2022) 154–180.
[107] C. Posch, T. Serrano-Gotarredona, B. Linares-Barranco, T. Delbruck, Proc. IEEE 102 (2014) 1470–1484.